

Paraiso : An Automated Tuning Framework for Explicit Solvers of Partial Differential Equations

Takayuki Muranushi

Hakubi Center for Advanced Research / Yukawa Institute for Theoretical Physics,
Kyoto University Kitashirakawa Oiwakecho, Sakyo-ku, Kyoto 606-8502 Japan

E-mail: muranushi.takayuki.3r@kyoto-u.ac.jp

Abstract.

We propose Paraiso, a domain specific language embedded in functional programming language Haskell, for automated tuning of explicit solvers of partial differential equations (PDEs) on Graphic Processing Units (GPUs) as well as multicore CPUs. In Paraiso, one can describe PDE solving algorithms succinctly using tensor equations notation. Hydrodynamic properties, interpolation methods and other building blocks are described in abstract, modular, re-usable and combinable forms, which lets us generate versatile solvers from little set of Paraiso source codes.

We demonstrate Paraiso by implementing a compressive hydrodynamics solver. A single source code less than 500 lines can be used to generate solvers of arbitrary dimensions, for both multicore CPUs and GPUs. We demonstrate both manual annotation based tuning and evolutionary computing based automated tuning of the program.

PACS numbers: 02.60.Cb, 02.60.Pn, 07.05.Bx

Keywords: 68N15 Programming languages, 68N18 Functional programming and lambda calculus, 65K10 Optimization and variational techniques, 65M22 Solution of discretized equations

1. Introduction

Today, computer architectures are becoming more and more complex, making it more and more difficult to predict the performance of a program before running it. Parallel architectures, GPUs being one example and distributed memory machines another, forces us to program in different ways and our programs tend to become longer. Moreover, to optimize them we are asked to write many different implementations of such programs, and the coding task becomes time-consuming. However, if we describe the problem we want to solve in a domain-specific language (DSL) from which a lot of possible implementations are generated and benchmarked, we can automate the tuning processes.

Examples of such automated-tuning DSL approaches are found in fast Fourier transformation library FFTW [1], linear algebra library ATLAS [2], digital signal processing library SPIRAL [3]. In these works the authors regarded automated tuning not just as a tool to avoid manual tuning, but as a necessary tool to have “portable performance” — the practical way of optimizing domain-specific codes for various complicated architecture we have today and in the future.

Now, our domain is explicit solvers of partial differential equations (PDEs). The main portions of such solvers consist of stencil computations, and a few global reduction operations needed to calculate Courant-Friedrichs-Lewy (CFL) conditions. Stencil computations are computations that update mesh structures, and the next state of a mesh depends only on the states of its neighbor meshes. Due to its inherent and coherent parallelism, stencil computation DSLs have been actively studied. For example, [4] have demonstrated $\times 1.5 - \times 5.6$ speedup on various hardwares via hardware and memory-hierarchy aware automated tuning. [5] have demonstrated generating multi-GPU codes that weakly scales up to 256 GPUs.

Still, reports are limited to simple equations such as diffusion equations and Jacobi solvers of Poisson equations, and to implement solvers of more complicated equations such as compressive hydrodynamics, magneto-hydrodynamics or general relativity, and their higher-order versions, we are forced to manually decompose the solving algorithms to imperative instructions that are often tens and hundred thousands of lines.

It is a problem common to all the languages that is designed to be compatible with C or Fortran, such as OpenMP, CUDA, PGI Fortran and OpenACC — that it is hard, if not impossible at all, to avoid repeating yourself in these languages. Despite all the efforts made so far to extend these languages, the programs in those languages fundamentally lack the ability to manipulate programs themselves and other abstract concepts. Every time a new generation of language appear, we are forced to make painful choices of porting a huge amounts of legacy codes to the new language. It is also a pain that various numerical techniques are mixed in one code, and can hardly be reused. If we want to make computers automatically combine such numerical techniques, compose a variety of implementations, and search for the better ones, the abstraction power is necessary. A complementary approach is needed here, that works together with the

parallel languages.

Our contribution, Paraiso (**PAR**allel **A**utomated **I**ntegration **S**cheme **O**rganizer), enables us describe PDE-solving algorithms succinctly using algebraic concepts such as tensors. Paraiso also enables us to describe various manipulations on algorithms such as introducing higher-order interpolations, in composable and reusable manner. That is, once we define a certain interpolation method in our language as a transformation of basic solver to a higher-order one, we can reuse the transformation for any equations. In this way Paraiso reduces the cost of rewriting when we search for better discretizations or interpolations; enables us to port the collections of algorithms to new parallel languages, without changing the Paraiso source codes but by updating the common code generator; allows yet another layer of automated tuning at translating Paraiso codes to other parallel languages.

In writing Paraiso, we wanted to define arithmetic operations between tensors and code generator fragments. We want our tensors to be polymorphic, but we don't want to allow addition between tensors of different dimensions. We wanted to make generalized functional applications. We wanted to traverse over data structures. We need to manage various contexts, like context of code generation and the context of serialization from a program to a genome.

Programming language Haskell supports all of these. Moreover, they are supported *not* as built-in features that users cannot change; they are libraries that Haskell users can freely combine or create their own. This flexibility of Haskell is based on its strong, static, higher-order type system with type classes and type inference. Thus Haskell essentially allows us to develop our own type-systems within it, which gives it a unique advantage as a platform for developing embedded DSLs. Many parallel and distributed programming languages has been implemented using Haskell [6]. Nepal[7] and Data Parallel Haskell [8] are implementations of NESL, a language for operating nested arrays in Haskell. Accelerate [9] and Nikola [10] are languages to manipulate arrays on GPUs written in Haskell. Finally, Liszt [11] is a DSL for solving mesh-based PDEs based on functional programming language Scala.

Our contributions are the following:

- A domain-specific language (DSL) embedded in Haskell, with which one can describe explicit solvers of partial differential equations (PDEs) in a succinct and organized manner, using tensor notations.
- A code-generation mechanism that takes the DSL and generates OpenMP and CUDA programs.
- A compressible Euler equations solver implemented in the DSL, and tuning experiments using the solver. Written in tensor notations, the solver can be applied to problems of arbitrary dimension without changing the source code at all but a single type declaration that sets the dimension of the solver.
- An annotation mechanism with which one can give hints to code generators, which makes it drastically easy to search for better implementations manually. By adding

just one line of hint to the solver causes overall refactoring, adding 4 subroutines to the generated code, making it consume 1.3 times more memory but 6.42 times faster.

- An automated benchmarking and tuning mechanism based on parallel simulated annealing and genetic algorithms, which generates a lot of different implementations of the PDE solvers and search for faster implementations. It speeds up the unannotated solver by factor of 5.26, and the annotated solver further by factor of 1.78.

Just for a comparison, the Paraiso framework is about 5'000 lines of code in Haskell, and the compressible Euler equations solver implemented in Paraiso is less than 500 lines. From that, we have generated more than 500'000 instances of the solver, each being 3'000 - 10'000 lines of code in CUDA. The automatically tuned codes are faster than the manually tuned codes reported by other groups. Paraiso is ready to optimize solvers of other equations, and all the solvers written in Paraiso can migrate to new parallel languages and new hardwares once the Paraiso code generator supports them.

Our work, Paraiso is the first consistent system that combine those previously studied techniques of symbolic computations, DSLs, GPU computations and automated tuning. We demonstrate the utility of such a system in the domain of explicit solvers of PDEs.

This paper is organized as follows. In section 2, we describe the overall design of Paraiso as well as its components. In section 3, we describe our automated tuning mechanism, which is a combination of genetic algorithm and simulated annealing that is designed to utilize the varying number of available nodes in a shared computer system. In section 4, we introduce the compressible hydrodynamics solver we choose as the tuning target, and describe the manual and automated tuning experiments. In section 5, we analyze the automated tuning history. In section 6 are concluding remarks and discussions.

2. The Design of Paraiso

2.1. Overall Design

Paraiso is to tackle the ambitious problem of generating fast and massively-parallel codes from human-friendly notations of algorithms. To divide the problem into major components, which may be conquered by different set of people, we set the overall design of Paraiso, as illustrated in Fig. 1.

The users of Paraiso must manually invent a discretized algorithm for the partial differential equations they want to solve. The solving algorithms are described in Paraiso using `Builder Monads`. `Builder Monads` generate programs for `Orthotope Machine (OM)`, a virtual parallel machine designed to denote parallel computations on multi-dimensional arrays. Then the back end OM compiler generates the native machine

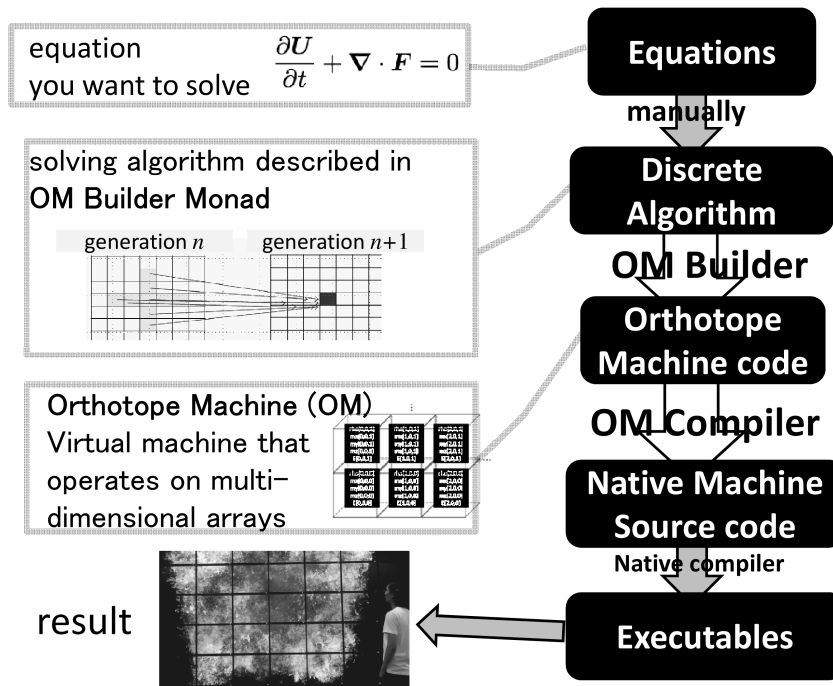


Figure 1. The Overall Picture.

source codes such as C++ and CUDA. Finally, native compilers translate them to executable codes.

When someone translates a simulation algorithm in his mind, to different languages such as Fortran, C and CUDA, he starts from building mathematical notations in his mind, and then gradually decomposes it to machine level. There should be the last common level that is independent of the detail of the target languages or the target hardwares. The level consist of very primitive operations on arrays. Orthotope Machine (OM) is designed to capture this level: The instruction set of the OM is kept as compact as possible, while maintaining all the parallelisms found in the solving algorithms. In forthcoming technical report we plan to provide the formal definition of the Orthotope Machine.

In order to generate the OM data-flow graphs from tensor expressions, and to translate them as native programs and further to apply manual and automated tuning over them, Paraiso introduces a number of abstract concepts centered around the OM. These components are quite orthogonal to each other, and some may even be useful outside the context of Paraiso. Table 1 summarizes those concepts, and provides pointers to the source code and the sections in this paper.

Orthotope Machine will endure the change in parallel languages and hardwares, as long as there are needs for explicit solvers of PDEs. Language/hardware designers can access to various applications for test and practical purpose, once they support translation from Orthotope Machine to their language. With Orthotope Machine as an

Name and Module	Description
<code>data ~, data Vec,</code> <code>class Vector, class VectorRing</code> in <code>Data.Tensor.TypeLevel</code>	Tensor algebra library that provides type level information for the tensor rank and dimension. c.f. §2.4.
<code>type Builder</code> in <code>Language.Paraiso.OM.Builder</code>	The Builder Monad for constructing the data flow graphs for OMs. c.f. §2.5.
<code>data OM</code> in <code>Language.Paraiso.OM</code>	The Orthotope Machine(OM), a virtual machine with basic instructions for stencil computations and reductions. c.f. §2.2.
<code>type Graph</code> in <code>Language.Paraiso.OM.Graph</code>	The data-flow graph for the OM. c.f. §2.2, Fig. 2, Fig. 3.
<code>type Annotation</code> in <code>Language.Paraiso.Annotation</code>	The collection of annotations that are added to each OM data-flow graph node. c.f. §2.6, §3.1.
<code>data Plan</code> in <code>Language.Paraiso.Generator.Plan</code>	The fixed detail of the code to be generated such as amount of memories and what to do in each subroutine. c.f. Fig. 5. To see how a plan is fixed c.f. Fig. 7.
<code>data Program</code> in <code>Language.Paraiso.Generator.Claris</code>	The subset of C++ and CUDA syntax tree which is sufficient in generating codes in scope of Paraiso. c.f. Fig. 5.
<code>newtype Genome</code> in <code>Language.Paraiso.Tuning.Genetic</code>	The set of annotations that belongs to an individual encoded as a string of letters, with which one can <code>mutate</code> , <code>cross</code> and <code>triangulate</code> . The evolution algorithm is in §3.2.

Table 1. List of concepts introduced by our work.

interface, we can combine various stencil computation applications with state-of-the-art techniques developed so far, such as cache-friendly data structures [4], overlapping communication with computation [12, 5] or heterogeneous utilization of CPU/GPU [13]. On the other hand, various concepts of numerical simulations has been decomposed to elemental calculations before the OM level, so the problem of how to build a parallel computation from components such as new spatial interpolations, time marching methods and approximate Riemann solvers, can be addressed and developed separately from the detail of the hardware. To achieve such orthogonality is one of the aims of the Paraiso project.

2.2. Outline of The Orthotope Machine(OM)

The Orthotope Machine (OM) is a virtual machine much like vector computers. Each register of OM is multidimensional array of infinite size. Arithmetic operations of OM work in parallel on each mesh, or loads from neighbor cells. We have no intention of building a real hardware: OM is a thought object to capture parallel algorithms to data-flow graphs without losing parallelism.

The instruction set of OM resembles those of historical parallel machines such as PAX computer [14], and is subset of partitioned global address space (PGAS) languages such as XcalableMP [15].

Each instance of OM have a specific dimension (e.g. a two-dimensional OM of size $N0 \times N1$). The variables of OM are either arrays of that dimension, or a scalar value. All of the arrays must have a common size. The actual numbers ($N0, N1$) are fixed at native code generation phase. We say that arrays are variable with `Local Realm`, while the scalars are variable with `Global Realm`.

OM has a set of `Static` variables which denotes the current state of the simulation. Each `Static` variable has a string name. OM has a set of `Kernels` — they are subroutines for updating the `Static` variables. Inside each `Kernel`, you can generate `Temporal` values in static single assignment (SSA) manner.

To summarize, the lifetime of an OM variable is either `Static` or `Temporal`, and the `Realm` of an OM variable is either `Local` or `Global`. `Static` variables survive multiple `Kernel` calls, while `Temporal` variables are limited to one `Kernel`. `Local` variables are arrays. `Global` variables are scalar values; in other words, they are arrays whose elements are globally the same.

OM cannot handle array of structures; `Local` variables may contain only simple objects such as `Bool` or `Double`, but not composite ones such as complex numbers or vectors. Nevertheless we can easily use such composite concepts in Paraiso programs at `Builder Monad` level and translate them to OM instructions, for example by using the applicative programming style [16].

An OM `Kernel` is a directed bipartite graph consisting of `NInst` nodes and `NValue` nodes, as illustrated in Fig. 2. Each node has `arity :: a -> (Int, Int)`, number of incoming and outgoing edges. `NValue` nodes have arity of $(1, n)$, where n is the number of `NInst` nodes that uses the value and can be an arbitrary integer. Arities of `NInst` nodes are inherited from the instructions they carry.

OM has nine instructions:

```
data Inst vector gauge
= Imm Dynamic
| Load StaticIdx
| Store StaticIdx
| Reduce R.Operator
| Broadcast
| Shift (vector gauge)
| LoadIndex (Axis vector)
| LoadSize (Axis vector)
| Arith A.Operator
```

Here, we limit ourselves to C pseudo-code of OM instruction semantics. The formal definition of the OM will be in forthcoming technical reports. Note that we do not translate the OM instructions one by one to C codes listed here. Instead, the instructions

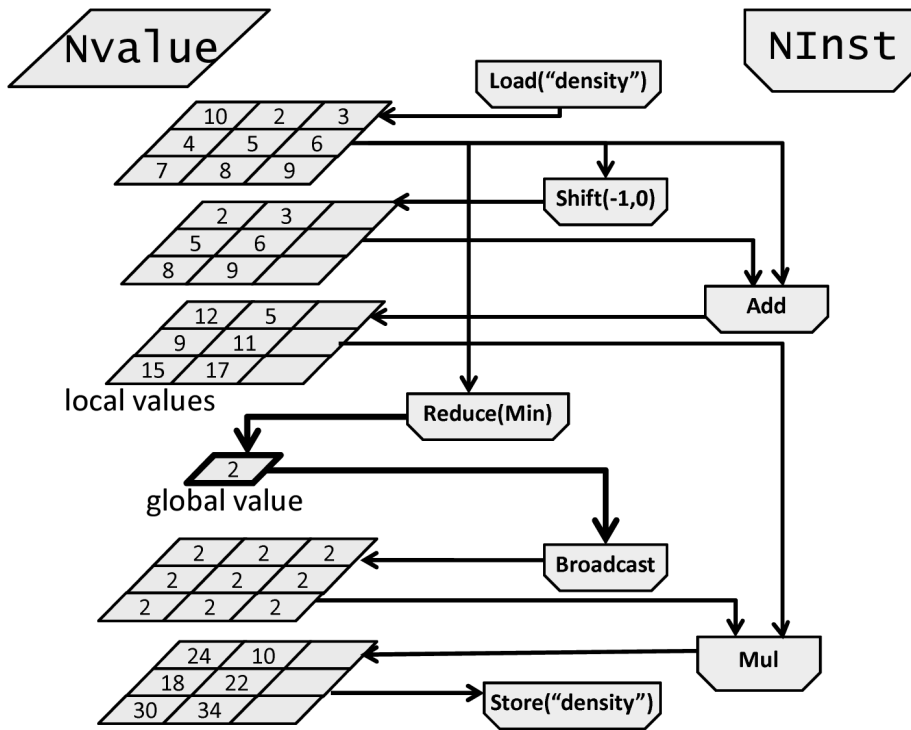


Figure 2. A data-flow graph for Orthotope Machine(OM).

are merged into sub-graphs and then translated to C loops (or CUDA kernels) with much larger bodies, to make efficient use of computation resource and memory bandwidth (c.f. §3.1).

Imm arity (0, 1): load constant value. Its output can be either **Global** or **Local NValue** node. For example, for a **Local Temporal** variable *a*,

```
a <- imm 4.2
```

means

```
for(int j=0; j<N1; ++j) {
  for(int i=0; i<N0; ++i) {
    a[j][i] = 4.2;
  }
}
```

Load arity (0, 1): read from static variable to temporal variable. The realms of the static and temporal variable must match, and can be either of **Global** or **Local**. For example, for a **Local Temporal** variable *a* and **Local Static** variable *density*,

```
a <- load "density"
```

means


```

for(int j=0; j<N1; ++j) {
  for(int i=0; i<N0; ++i) {
    a[j][i] = density[j][i];
  }
}

```

Store arity (1,0): write a temporal variable to a static variable. The realms of the static and temporal variable must match, and can be either of **Global** or **Local**.

```
store "density" <- a
```

means

```

for(int j=0; j<N1; ++j) {
  for(int i=0; i<N0; ++i) {
    density[j][i] = a[j][i];
  }
}

```

Reduce arity (1,1): convert a local variable to a global one with a specified reduction operator.

```
b <- reduce Min <- a
```

means

```

b = a[0][0];
for(int j=0; j<N1; ++j) {
  for(int i=0; i<N0; ++i) {
    b = min(b,a[j][i]);
  }
}

```

Broadcast arity (1,1): convert a global variable to a local one.

```
b <- broadcast <- a
```

means

```

for(int j=0; j<N1; ++j) {
  for(int i=0; i<N0; ++i) {
    b[j][i] = a;
  }
}

```

Shift arity (1,1): takes a constant vector and an input local variable. Move each cell to its neighbor.

```
b <- shift (1,5)<- a
```

means

```
for(int j=0; j<N1-5; ++j) {
  for(int i=0; i<N0-1; ++i) {
    b[j+5][i+1] = a[j][i];
  }
}
```

LoadIndex arity (0,1): get coordinate of each cell. The output must be a **Local** value.

```
b0 <- loadIndex 0
```

```
b1 <- loadIndex 1
```

means

```
for(int j=0; j<N1; ++j) {
  for(int i=0; i<N0; ++i) {
    b0[j][i] = i;
  }
}
for(int j=0; j<N1; ++j) {
  for(int i=0; i<N0; ++i) {
    b1[j][i] = j;
  }
}
```

LoadSize arity (0,1): get array size. The output must be a **Global** value.

```
c0 <- loadSize 0
```

```
c1 <- loadSize 1
```

means

```
c0 = N0;
```

```
c1 = N1;
```

Arith perform various arithmetic operations. The arity of this **NInst** node is inherited from its operator. The realms of the inputs and outputs must match, and can be either of **Global** or **Local**. If **Local**, array elements at matching index are operated in parallel (i.e. `zipWith`).

For example,

```
c <- arith Add a b <- a,b
```

means

```
for(int j=0; j<N1; ++j) {
  for(int i=0; i<N0; ++i) {
    c[j][i] = a[j][i] + b[j][i];
  }
}
```

2.3. An Example of Orthotope Machine Data-Flow Graph

Here we show the use case of the Orthotope Machine operators introduced in §2.2 within a simple PDE solver. We solve the following linear wave equation:

$$\frac{\partial^2 f}{\partial t^2} - c^2 \frac{\partial^2 f}{\partial x^2} = 0, \quad (1)$$

where t is time, x is one-dimensional space coordinate and c is the signal speed.

By introducing the time derivative $g = \partial f / \partial t$, Eq. (1) is rewritten as following system of first-order PDEs:

$$\frac{\partial f}{\partial t} = g, \quad (2)$$

$$\frac{\partial g}{\partial t} = c^2 \frac{\partial^2 f}{\partial x^2}, \quad (3)$$

and satisfies the following conservation law:

$$\frac{d}{dt} E = 0, \quad (4)$$

$$E \equiv \int \left(\frac{c^2}{2} \left(\frac{\partial f}{\partial x} \right)^2 + \frac{g^2}{2} \right) dx. \quad (5)$$

We will write a Paraiso code that simulate the discrete system of Eqs. (2,3) and tests the conservation law.

Let $f^n[i]$ denote the discrete field where n and i are the discrete time and space coordinate, respectively. We choose the following 2nd-order, Lax-Wendroff and Leap Frog scheme to solve Eqs. (2,3) :

$$f^{n+1}[i] = f^n[i] + \Delta t g^n[i], \quad (6)$$

$$g^{n+1}[i] = g^n[i] + \frac{c^2 \Delta t}{\Delta x^2} (f^{n+1}[i+1] + f^{n+1}[i-1] - 2f^n[i]), \quad (7)$$

and measure the following discrete form of the conserved quantity:

$$E^{n+1} \equiv \sum_{i=0}^{N-1} \left[\left(\frac{c^2 f^{n+1}[i+1] - f^{n+1}[i-1]}{2 \Delta x} \right)^2 + \left(\frac{g^{n+1}[i] + g^n[i]}{2} \right)^2 \right] \Delta x \quad (8)$$

Table 2 shows the Paraiso implementation for the algorithm Eq. (6,7). The corresponding OM data-flow graph is visualized in Fig. 3. See how the data-flows

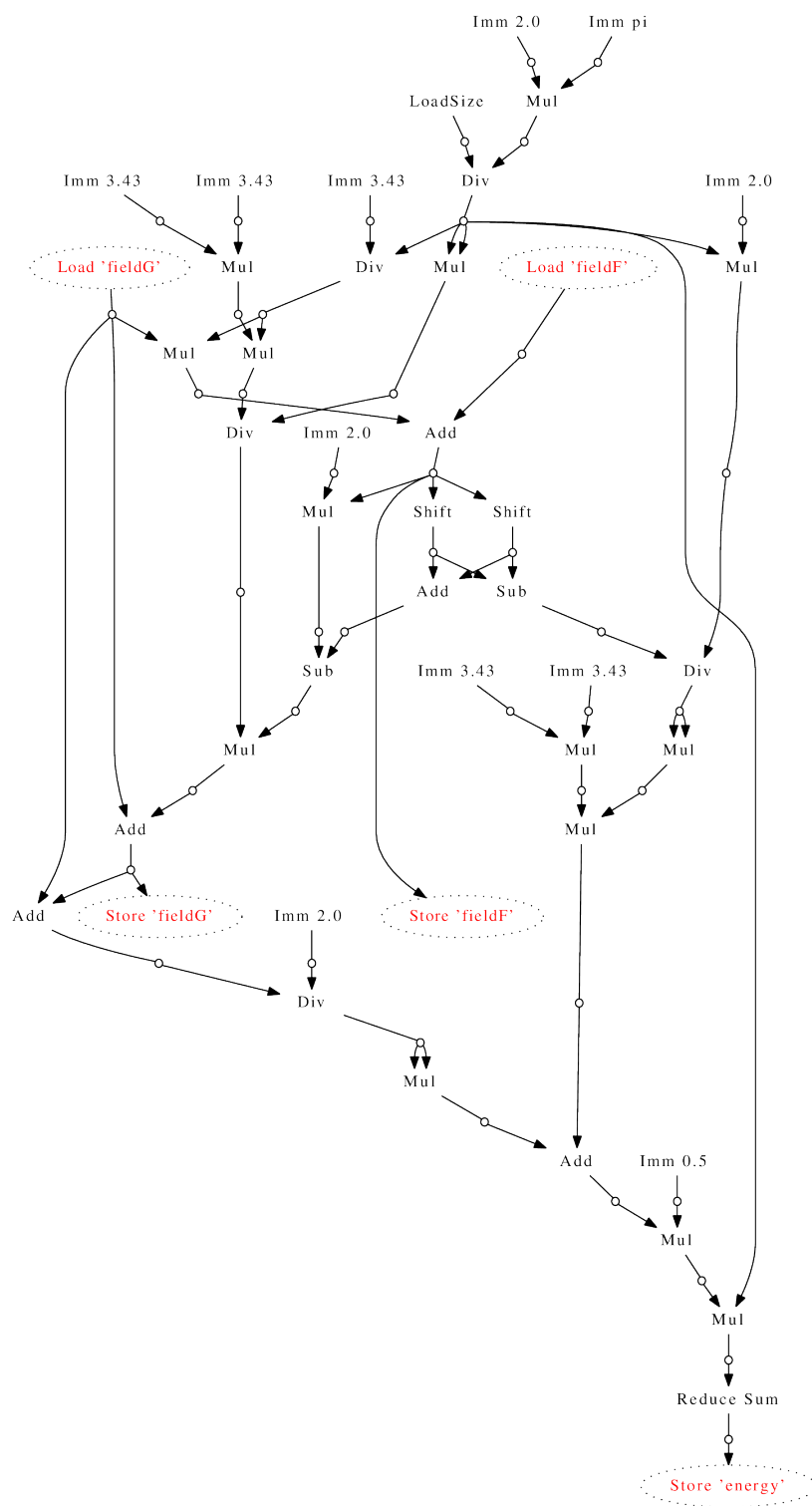


Figure 3. The Orthotope Machine data-flow graph generated from the Paraiso source code listed in Table 2. For brevity, NValue nodes are represented as little circles and only NInst nodes are shown; the Arith instruction nodes are replaced by arithmetic operators inside them, and the instruction arguments are not shown but for Load, Store and Reduce.

```

proceed :: Builder Vec1 Int Annotation ()
proceed = do
  c <- bind $ imm 3.43
  n <- bind $ loadSize TLocal (0::Double) $ Axis 0

  f0 <- bind $ load TLocal (0::Double) $ fieldF
  g0 <- bind $ load TLocal (0::Double) $ fieldG
  dx <- bind $ 2 * pi / n
  dt <- bind $ dx / c

  f1 <- bind $ f0 + dt * g0
  fR <- bind $ shift (Vec:~ -1) f1
  fL <- bind $ shift (Vec:~ 1) f1
  g1 <- bind $ g0 + dt * c^2 / dx^2 *
    (fL + fR - 2 * f1)
  store fieldF f1
  store fieldG g1

  dfdx <- bind $ (fR - fL) / (2*dx)
  store energy $ reduce Reduce.Sum $
    0.5 * (c^2 * dfdx^2 + ((g0+g1)/2)^2) * dx

```

Table 2. A Paraiso source code for solving discrete Eq. (6,7).

from `Load` node to `Store` node. Here, we have $c = 3.43$ and $0 \leq x < 2\pi$. We have performed numerical simulations using this program and the following initial condition:

$$f(x) = \sin(x), \quad (9)$$

$$g(x) = \cos(3x), \quad (10)$$

with resolution varying from $N = 8$ to $N = 3072$, and have confirmed that the fluctuation of discrete conserved quantity, Eq. (8) was smaller than of the order of 10^{-13} .

2.4. Typelevel Tensor

We introduce `typelevel-tensor` library, to abstract over the dimensions; the use of tensor notations allow us to describe the algorithms for different dimensions in a single source code. The benefit of having information on tensor dimensions and ranks at the type-level is that we can detect erroneous operations like adding two tensors of different dimensions at compile time. Also we have much less need for explicitly mentioning the tensor dimensions in our programs, because the dimensions will be type-inferred.

Our approach is similar to that in [17], where two constructors `Z` and `:.` are used to inductively define multi-dimensional tuples. Their n -dimensional vectors are actually n -tuples, so it is possible that the set of n elements consist of different types. In contrast,

we needed that all the n elements of a vector are of the same type, because we wanted to operate on them, for example by applying a same function to all of them.

So instead of [17]’s approach:

```
infixl 3 :.
data Z = Z
data tail :: head = tail :: head
```

We have these:

```
infixl 3 :~
data Vec a = Vec
data (n :: * -> *) :~ a = (n a) :~ a
```

Here, `Vec` is the type constructor for 0-dimensional vector, and `:~` is a type-level function that takes the type constructor for n -dimensional vector as an argument and returns the type constructor for $n + 1$ -dimensional vector. We define type synonyms for successively higher vector:

```
type Vec0 = Vec
type Vec1 = (:~) Vec0
type Vec2 = (:~) Vec1
type Vec3 = (:~) Vec2
```

`Vec0`, `Vec1`, `Vec2`, and `Vec3` are all types of kind `* -> *`, meaning that it takes one type (the element type) and returns another (the vector type). For example, the three-dimensional double precision vector type is `Vec3 Double`. Higher-rank tensors are defined as nested vectors; for example `Vec3 (Vec3 Int)` is a 3×3 matrix of integers.

Since we know that all the elements of our tensor are of the same type `a`, we can make our tensors instances of `Traversable` type class [16, 18]:

```
instance Traversable Vec where
  traverse _ Vec = pure Vec
instance (Traversable n) => Traversable ((:~) n) where
  traverse f (x :~ y) = (:~) <$> traverse f x <*> f y
```

The benefit of making our tensors instances of `Traversable` is that we can `traverse` on them:

```
traverse :: Applicative f => (a -> f b) -> t a -> f (t b)
```

Here, suppose `t` is our tensor type-constructor and `f` is some context — for example, a code generation context. `a` and `b` are elements of our tensor. Then the type of the `traverse` function means that if we have code generators for the computation of one element `(a -> f b)`, and we have a `t a`, a tensor whose elements are of type `a`, then we can deduce the code generator for computation of the entire tensor `f (t b)`.

2.5. Builder Monad

`Builder` monad is a `State` monad whose state is the half-built data-flow graph of the Orthotope Machine. To represent the data-flow graph, we use Functional Graph Library (FGL) [19, 20]. Authors learned from the `Q` monad [21] how to encapsulate the construction process.

The graph carried by the `State` monad has the following type:

```
type Graph (vector :: *->*) (gauge :: *) (anot :: *)
  = FGL.Gr (Node vector gauge anot) Edge
```

```
data Node vector gauge anot =
  = NValue DynValue anot
  | NInst (Inst vector gauge) anot
```

```
data Edge
  = EUnord
  | EOrd Int
```

`Graph` takes three type arguments. `vector :: *->*` is a type constructor that denotes the dimension of the OM. `gauge` is the type for the indices of the arrays, which is usually an `Int`. `anot` is the type the nodes of the graph are annotated with. Such annotations are used to analyze and optimize the data-flow graph.

The three types `vector`, `gauge`, and `anot` are passed to the `Nodes` of the graph. `Nodes` are either `NValue` or `NInst`. Two types `vector` and `gauge` are further passed to the instruction type `Inst`, because instructions such as `shift` requires the information on the array dimension and indices. Every graph nodes are also annotated by type `anot`.

On the other hand, the edges contain none of the three types. They are just unordered edges `EUnord` or edges ordered by an integer `EOrd Int`. For example, we can exchange two edges going into addition instruction, but cannot exchange those into subtraction.

We define various mathematical operations between `Builder Monad` in a consistent manner (c.f. Fig. 4). For any operator \oplus , `Builder A \oplus Builder B = Builder C` is defined by `Value A \oplus Value B = Value C`, where `Value i` is the value computed by `Program i` which is generated by `Builder i` . For example, a helper function that takes an operator symbol `op`, two builders `builder1` and `builder2`, and create a binary operator for builder, is as follows:

```
mkOp2 :: (TRealm r, Typeable c) =>
  A.Operator          -- ^The operator symbol
-> (Builder v g a (Value r c)) -- ^Input 1
-> (Builder v g a (Value r c)) -- ^Input 2
-> (Builder v g a (Value r c)) -- ^Output
mkOp2 op builder1 builder2 = do
```

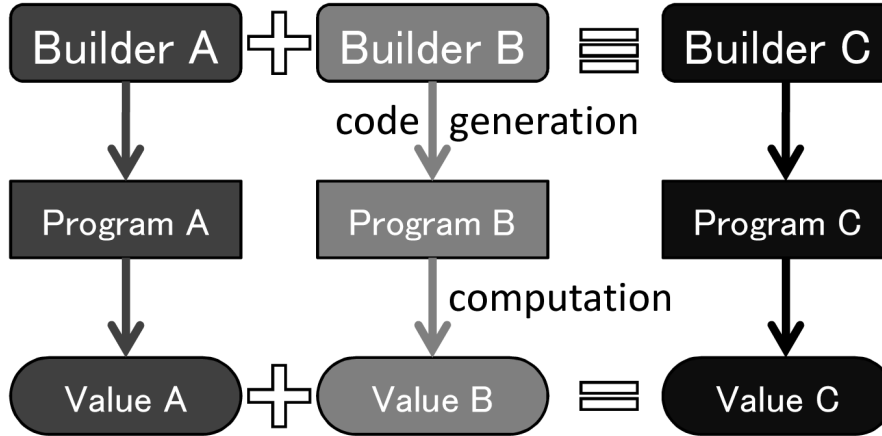


Figure 4. A commutative diagram of Builder Monad and computation.

```

v1 <- builder1
v2 <- builder2
let
  r1 = Val.realm v1
  c1 = Val.content v1
n1 <- valueToNode v1
n2 <- valueToNode v2
n0 <- addNodeE [n1, n2] $ NInst (Arith op)
n01 <- addNodeE [n0] $ NValue (toDyn v1)
return $ FromNode r1 c1 n01

```

We first extract the graph nodes from left hand side and right hand side builders in Builder context, add an NInst node that contains op symbol, add an NValue node after that, and return the node index.

In Haskell, defining mathematical operators between a data type is done by declaring the data type as an instance of the *type class* that manages the operator. In this sense type classes in Haskell are the parallels of algebraic structures such as group, ring and field, that manages addition, multiplication, and division, respectively. We use a Haskell package `numeric-prelude` that provides such algebraic structures [22].

For example, an Additive instance declaration of Builder is as follows:

```

instance (TRealm r, Typeable c, Additive.C c)
=> Additive.C (Builder v g a (Value r c)) where
zero = return $ FromImm unitTRealm Additive.zero
(+) = mkOp2 A.Add
(-) = mkOp2 A.Sub
negate = mkOp1 A.Neg

```

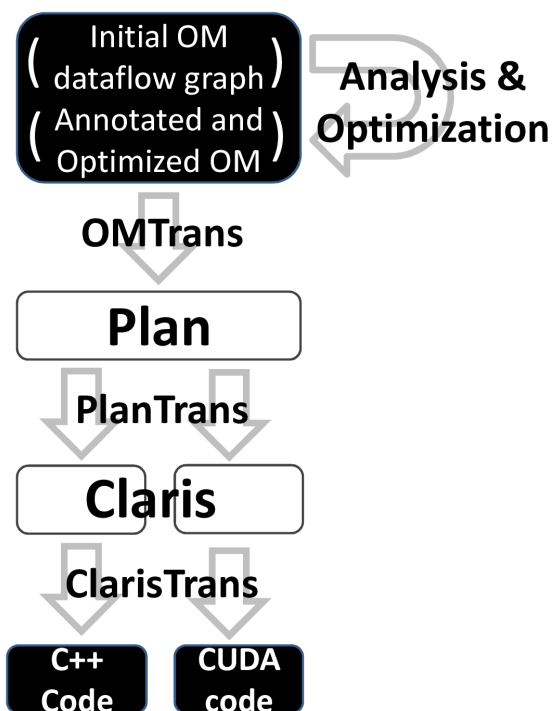



Figure 5. Backend.

These type class instances, together with typelevel-tensor library, allows us to write tensor equations used in Paraiso application programs. Moreover, such equations are good for arbitrary instances of the type class. For example, here are the definition of momentum and momentum flux in our Euler equations solver:

```

momentum x = compose (\i -> density x * velocity x !i)
momentumFlux x =
  compose (\i -> compose (\j ->
    momentum x !i * velocity x !j + pressure x * delta i j))
  
```

These functions can be used to directly calculate momentum vector and momentum flux tensor whose components are of type `Double`. The very same functions are used to generate the solvers for CPUs and GPUs. At that time, their components are inferred to be `Builder` types. In addition to that, these functions can handle tensors of arbitrary dimensions.

2.6. Backend

The back end converts the data-flow graph of `Kernel`s native codes, and create a C++ class corresponding to an OM. The code generation processes of Paraiso is illustrated in Fig. 5.

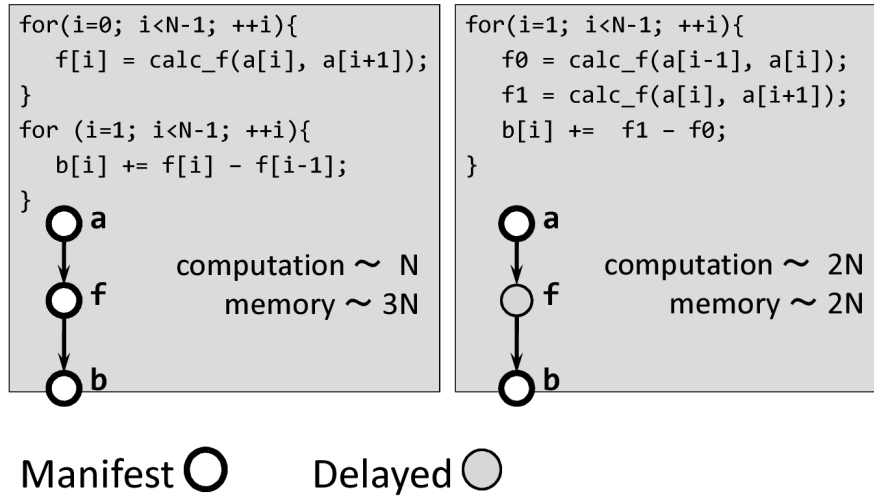


Figure 6. A Manifest - Delayed trade off. The left code requires less arithmetic units but consumes more memory and its bandwidth; The right code requires less memory and bandwidth in cost of more computations.

First, various analysis and optimizations are applied. Analysis and optimizations are functions that takes an OM and returns an OM, so we can combine them in arbitrary ways. Though some analysis are mandatory for code generation.

Paraiso has an omnibus interface for analysis and optimization using dynamic programming library `Data.Dynamic` in Haskell [23] :

```

type Annotation = [Dynamic]
add :: Typeable a => a -> Annotation -> Annotation
toList :: (Typeable a) => Annotation -> [a]
toMaybe :: (Typeable a) => Annotation -> Maybe a

```

Here, analyzers as well as human beings can add annotations of arbitrary type `a` to the graph. On the other hand, optimizers can read out annotations of what type they recognize and perform transformations on the data-flow graph. The set of annotations can be serialized to, and deserialized from *genomes*, which are binary strings used in automated tuning phase.

Examples of annotations are the choices of whether to store a value on memory and reuse or not to store and recompute it as is needed (c.f. Fig. 6); the boundary analysis result used for automatically adding ghost cells; dependency analysis; and labels used for dead code eliminations.

Once the analysis and optimizations are done, an OM is translated to a code generation `Plan`. Here, decisions are made for how many memory are used, what portion of computation goes into a same subroutine, and so on. The nodes in data-flow graph are greedily merged as long as they have no dependence and can be calculated in the

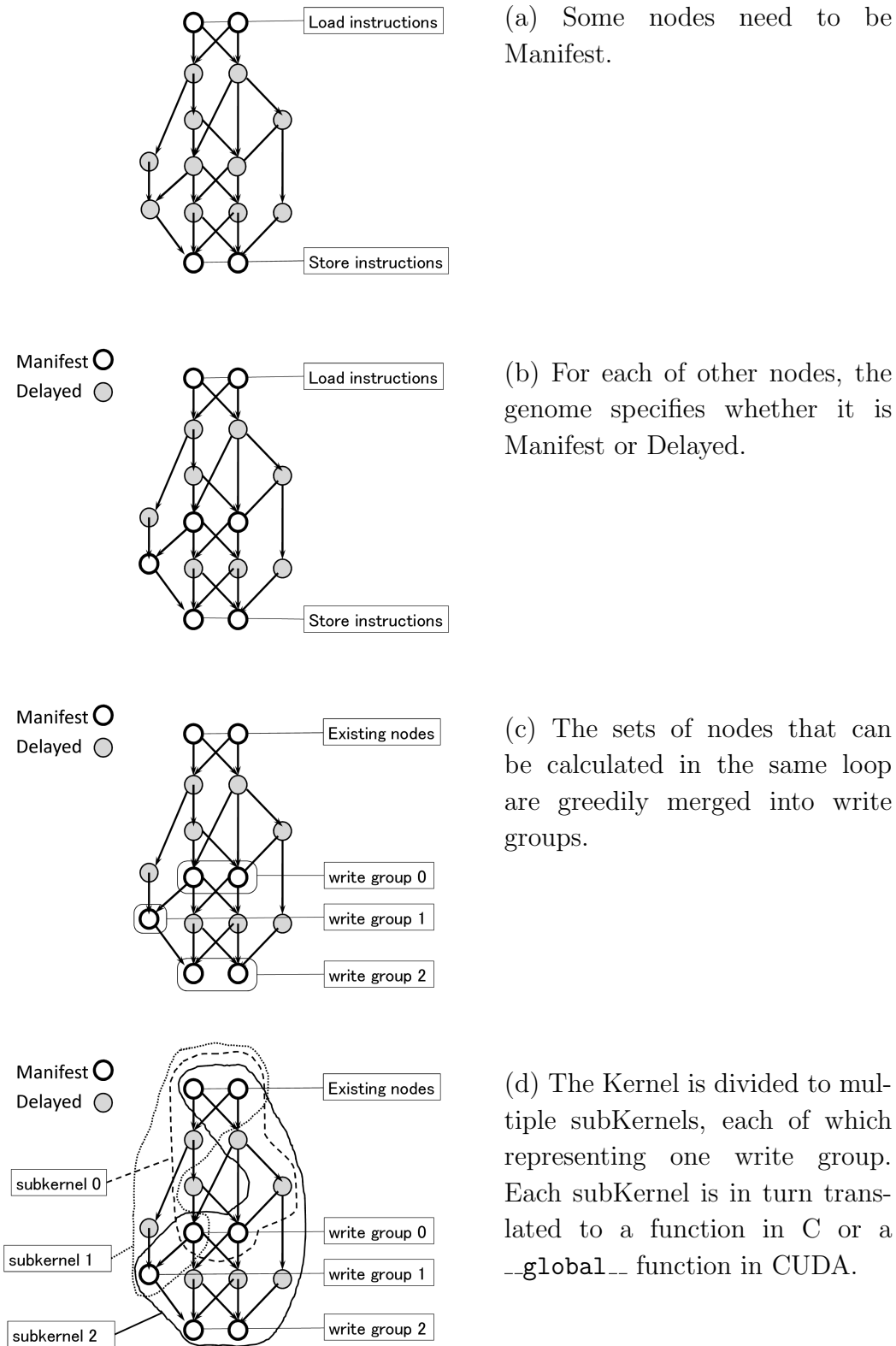


Figure 7. How Paraiso generates a Plan from the given set of annotations.

same loop (Fig. 7).

The `Plan` is further translated to `CLARIS` (C++-Like Abstract Representation of Intermediate Syntax). `CLARIS` is subset of C++ and CUDA syntax which is sufficient in generating codes in scope of Paraiso.

Finally, `CLARIS` is translated to native C++ or CUDA codes.

3. Automated Tuning Mechanism

3.1. Tuning Targets

The objects we want to optimize are the implementations of a partial differential equations solving algorithm. We call them *individuals*, adopting the genetic algorithm terminology. Each individual has a *genome* that encodes how it have chosen to implement the algorithm. The choices are (1) how much computation speed and memory bandwidth to use, (2) where to synchronize the computation, and (3) the CUDA kernel execution configuration. The fitness of the genome is the benchmark score of the generated code, measured in cups (the number of fluid cells updated per second) which we want to maximize.

A simple example program Fig. 6 indicates that we have implementation choices for intermediate variables: whether to store its entire contents on the memory (`Manifest`) or not to store them and recompute them as they're needed (`Delayed`). The terms `Manifest` and `Delayed` are inherited from REPA [17]. If we increase the number of `Manifest` nodes, we consume less arithmetic units but more memory and its bandwidth; decreasing the number of `Manifest` nodes have the opposite effect. There are two extreme configurations, one is making as many nodes `Manifest` as possible and the other is making as few nodes `Manifest` as possible. In most cases both of them result in poor performance and moderate configurations are faster. Paraiso generate codes for many possible combinations of `Manifest` / `Delayed` choices (Fig. 7) and searches for such configurations by automated tuning.

Another tuning done by Paraiso is the choice of synchronization points. In CUDA, inserting `--syncthreads()`, especially before load/store instructions cause the next instruction to coalesce and increase the speed of the program. Inserting too much synchronization, on the other hand, is a waste of time. Again, Paraiso searches for better configurations by automated tuning.

The last tuning done by Paraiso is to find the optimal CUDA kernel execution configuration, i.e. how many CUDA threads and thread blocks to be launched simultaneously. These tuning items summed, the genome size is approximately 6000 bits for our hydrodynamics solver, which means that there are 2^{6000} possible implementations. Brute-force searching for *the* fastest implementation from this space is inutile and in the first place impossible. Instead, the goal of Paraiso is to stochastically solve such a global optimization problem in this genome space, where the function to be optimized is the benchmark score of the PDE solver generated from the genome.

```

proceed = do
  x <- bind $ loadLD density

  y <- bind $ x * x

  z <- bind $ y + y
  store density z

```

```

proceed = do
  x <- bind $
    Anot.add Sync.Pre <?>
    loadLD density
  y <- bind $
    Anot.add Alloc.Manifest <?>
    x * x
  z <- bind $ y + y
  store density z

```

Their genome:

AAAAACAAAAAAAAACAAAAAA

AAAAACAAAAAAAAACAACGAA

The generated header file, abbreviated:

```

class Hello {
public:device_vector<double> static_0_density;
public:device_vector<double> manifest_0_5;

public:void Hello_sub_0
  (const device_vector <double> &a1,
   device_vector <double> &a5);

public:void proceed ();
};

```

```

class Hello {
public:device_vector<double> static_0_density;
public:device_vector<double> manifest_0_3;
public:device_vector<double> manifest_0_5;

public:void Hello_sub_0
  (const device_vector<double> &a1,
   device_vector < double >&a3);
public:void Hello_sub_1
  (const device_vector<double> &a3,
   device_vector<double> &a5);
public:void proceed ();
};

```

The generated .cu program file, abbreviated:

```

__global__ void Hello_sub_0_inner
(const double *a1, double *a5) {
  for (int i = INIT; i < (256);
       (i) += STRIDE) {
    int addr_origin = i;
    double a1_0 = (a1)[(addr_origin) + (0)];
    double a3_0 = (a1_0) * (a1_0);
    ((a5)[addr_origin]) = ((a3_0) + (a3_0));
  }
}

void Hello::proceed () {
  Hello_sub_0 (static_0_density, manifest_0_5);

  (static_0_density) = (manifest_0_5);
}

```

```

__global__ void Hello_sub_0_inner
(const double *a1, double *a3) {
  for (int i = INIT; i < (256);
       (i) += STRIDE) {
    int addr_origin = i;
    __syncthreads ();
    double a1_0 = (a1)[(addr_origin) + (0)];
    ((a3)[addr_origin]) = ((a1_0) * (a1_0));
  }
}

__global__ void Hello_sub_1_inner
(const double *a3, double *a5) {
  for (int i = INIT; i < (256);
       (i) += STRIDE) {
    int addr_origin = i;
    double a3_0 = (a3)[(addr_origin) + (0)];
    ((a5)[addr_origin]) = ((a3_0) + (a3_0));
  }
}

void Hello::proceed () {
  Hello_sub_0 (static_0_density, manifest_0_3);
  Hello_sub_1 (manifest_0_3, manifest_0_5);
  (static_0_density) = (manifest_0_5);
}

```

Table 3. An example of changes in the genome and the implemented algorithm caused by annotations.

Table 3 shows a simple Paraiso kernel and how its genome and implementation is altered by adding annotations. This kernel named `proceed` performs the following calculations:

$$\begin{aligned}
 &\text{foreach } \mathbf{i} : \\
 &\quad x = \text{density}[\mathbf{i}] \\
 &\quad y = x \times x \\
 &\quad z = y + y \\
 &\quad \text{density}[\mathbf{i}] = z
 \end{aligned} \tag{11}$$

It first loads from an array named `density`, performs a multiplication, then an addition, and then stores the result to `density` again.

The header file on the right side of the Table 3, compared to the left one, allocates an additional `device_vector` and declares an additional subkernel as results of a `Manifest` annotation. The right `.cu` file, compared to the left one, differs in two points: one is that it performs the multiplication $y = x * x$ and the addition $z = y + y$ in separate CUDA kernels and stores the intermediate result to the additional `device_vector`, which is yet another result of the `Manifest` annotation. Another difference is that it calls `__syncthreads()` just before the load instruction, which is the result of the synchronization annotation.

3.2. Parallel Asynchronous Genetic Simulated Annealing

Simulated annealing has been widely used to solve global optimization problems. However, a standard simulated annealing method is not suitable for parallelization, and if the annealing schedule (how we cool down the temperature as function of time) is too quick, it tends to fall into local minima. Replica-exchange Monte Carlo method [24] solves these drawbacks by introducing multiple replicas of heat baths with different temperatures, and by allowing replica exchange between adjacent heat baths. Thus, replicas can be computed in parallel, and the annealing schedule is spontaneously managed by replica migration.

We further extend this method to fit into benchmark based tuning on shared cluster computer systems. First, in shared systems it is hard to maintain a fixed number of replicas because the available amount of nodes changes with time. Second, it is not efficient to perform replica-exchange synchronously, since the wall clock time required to calculate the fitness function varies with replicas. For these two reasons, we modify replica-exchange Monte Carlo method to a master/worker model (c.f. Fig. 8), where a master asynchronously launches varying number of workers in parallel.

The master holds the genomes and scores of all the past individuals in a database (DB). The role of the master is to draw individuals from the DB, to create new individuals using their genomes, and to launch the workers when the computer resource is available. The role of the workers, on the other hand, is to generate codes from the given genome, to take the benchmark, and to write the results into the DB.

In this way we can launch any number of workers asynchronously as long as the DB

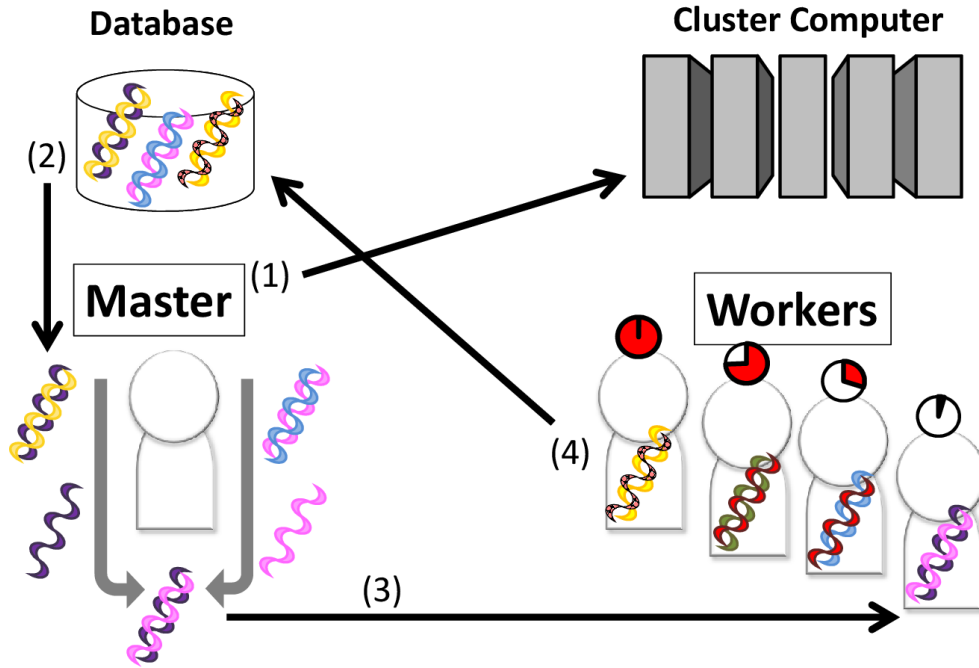


Figure 8. The master/worker model of parallel asynchronous genetic simulated annealing used for automated tuning in Paraiso. (1) The master periodically monitors for vacancy in the cluster computer system. (2) When a vacancy is found, the master creates a new individual from several genomes obtained from the database by performing *draws* of temperature T . (3) The master creates a worker job that generates native program from the genome and measures its speed. (4) Each worker writes the benchmark result to the database and quit as soon as it finishes its assigned measurements.

is not a bottleneck. In addition to that, we eliminate a common weak point of simulated annealing and genetic algorithms — that individuals of older generation are overwritten and are inaccessible.

For each individual I , the generated code is benchmarked 30 times. We record the mean $\mu(I)$ and the sample standard deviation $\sigma(I)$ of the score. It is important to record the deviation. When we benchmark each individual only once, some individuals receive over-evaluated score by chance, infest the system and tend to stall the evolution.

At the end of each benchmark, the individual is briefly tested if the state of the simulation has developed substantially from the initial condition and there is no NaN (not a number). The test is chosen because not evolving at all and generating NaN are two dominant modes of failure, and the individual test time needs to be kept smaller than benchmark itself. If an individual fails a test, its score is 0. At the end of a tuning experiment, the champion individual is extensively tested if it can reproduce various analytic solutions, which takes hours.

A *draw* is the operation to randomly choose an individual from the DB. Each draw has a temperature T . In a draw of temperature T , the probability the individual I is

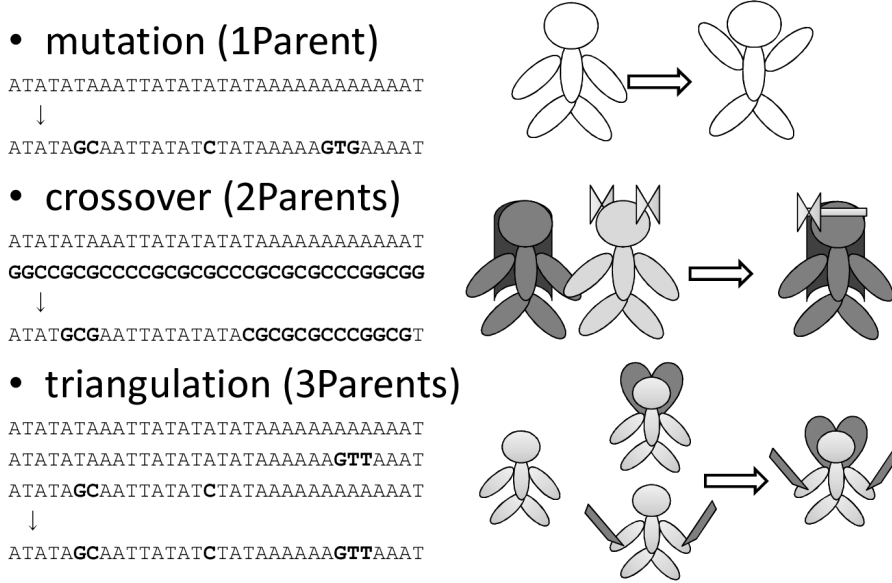


Figure 9. Three ways of generating new individuals.

chosen is proportional to

$$\exp\left(\frac{\mu(I_{\top}) - \mu(I) + \sigma(I_{\top}) + \sigma(I)}{T + \sigma(I_{\top}) + \sigma(I)}\right), \quad (12)$$

where I_{\top} is the individual with the largest $\mu(I)$.

Low-temperature draws strictly prefer high-score individuals while high-temperature draws does not care the score too much. And the difference small compared to $\sigma(I_{\top}) + \sigma(I)$ is gracefully ignored.

Every time master creates a new individual, it chooses the draw temperature T randomly, so that the probability density of $\log T$ is uniformly distributed between $\log(\sigma(I_{\top}))$ and $\log(\mu(I_{\top}))$.

To summarize, our method is a master/worker variant of replica-exchange Monte Carlo method [24], using genetic algorithms as neighbor generators. Thus, our method

- can utilize parallel and dynamically varying computer resource.
- can find global maximum without hand-adjusted annealing schedule.
- can combine independently-found improvements.

An extensive review on the applications of the evolutionary computation in astronomy and astrophysics is found in [25].

3.3. Three Methods of Birth for Generating New Individuals

We use three different methods of birth to generate new individuals (c.f. Fig. 9).

Base	0	0	0	0	1	1	1	1
Secondary	0	0	1	1	0	0	1	1
Primary	0	1	0	1	0	1	0	1
Child	0	1	1	1	0	0	0	1

Table 4. Binary operation table for triangulation.

The first method is *mutation*. We draw one individual from the database (DB), take its genome, overwrite it randomly and create a new genome. The second method is *crossover*. We draw two individuals from the DB, split their genomes at several random points and exchange the segments. The third method is *triangulation*, or three-parent crossover.

Multi-parent crossovers are crossovers that takes more than two parents and create one or multiple children. The proposed multi-parent crossover methods include taking bit-wise majority vote [26, 27] and exchanging segments between multiple parents [28]. Multi-parent crossovers for real-number coded genomes are also studied [29]. The novelty of our three-parent crossover (triangulation) is to take the scores of the parents into consideration. Triangulation is designed to efficiently combine independent improvement found in sub-problems.

FFTW [1] uses the divide and conquer approach to its target problems. It first recursively decomposes large FFT problem into smaller ones and solves the optimization problem from smaller part. In contrast, Paraiso deals with monolithic data-flow graphs. It is not obvious how to decompose them into subgraphs — decompositions are actually the target of optimization. Therefore, we optimize subgraphs in vivo; we optimize subgraphs keeping them embedded into the entire graph.

Aiming to merge two distinct optimized subgraphs, we draw three individuals from the DB. Then we sort them in ascending order of the score and name them **Base**, **Secondary** and **Primary**. We perform bit-wise operation as in Table 4 to create their child. For each bit, if at least one of **Primary** or **Secondary** has been changed from **Base**, then we adopt the change.

When creating a new individual, the master chooses mutation, crossover, or triangulation at equal probability of $1/3$. Then the master draws the needed number of parents from the DB. If two of the parents are the same the master retries the draws. Otherwise, the master creates a child with the chosen method of birth. Then if the genome of the newly created individual is already in the DB, the master discards the individual and retries the mutation until it gets a genome not found in the DB. With each retry, draw temperature T is multiplied by 1.2, so that the master eventually

succeed in creating a new genome.

4. Tuning Experiments

4.1. The Target Program

We implemented a 2nd order compressible hydrodynamics solver [30] in Paraiso, and then optimize it. Here we detail numerical scheme.

Let A_a, B_{ab}, \dots denote tensor indices for tensor A, B, \dots . Let $[\mathbf{i}], [\mathbf{j}], \dots$ denote array indices which is a d -tuple of integer where d is the dimension. Values integrated over cell volumes are given integer indices, and values integrated over cell surfaces are given indices with one half-integer and $d-1$ integers. For example, $A_y[\mathbf{i}]$ is the volume integral of y -component of a vector A over the cell \mathbf{i} , and $B_{xz}[\mathbf{i} + \frac{1}{2}\mathbf{e}_x]$ is the surface integral of xz -component of a rank-2 tensor B over the $+x$ surface of cell \mathbf{i} .

The equations of compressible hydrodynamics have $d+2$ degrees of freedom. The primitive variables \mathbf{V} and the conserved variables \mathbf{U} are the two representations of the degrees of freedom. The flux variables \mathbf{F} are calculated from \mathbf{U} or \mathbf{V} , as follows :

$$\mathbf{V} = \begin{pmatrix} \rho \\ v_a \\ p \end{pmatrix}, \quad (13)$$

$$\mathbf{U} = \begin{pmatrix} \rho \\ m_a \\ E \end{pmatrix}, \quad (14)$$

$$\mathbf{F}_a = \begin{pmatrix} u_a \\ u_a m_b + p \delta_{ab} \\ u_a E + u_a p \end{pmatrix}. \quad (15)$$

where ρ , v_a , m_a , p and E are the density, the velocity, the momentum, the pressure and the total energy, respectively, The primitive and conserved variables are related by $m_a = \rho v_a$, $E = E_i(p) + \frac{1}{2}\rho v^2$ where E_i is the internal energy of the gas. By assuming the adiabatic equation of state for perfect gas, $E_i(p) = (\gamma - 1)^{-1}p$ where γ is the ratio of specific heats.

We numerically solve the Euler equations $\partial_t \mathbf{U} = \partial_a \mathbf{F}_a$, or more specifically:

$$\partial_t \rho = \partial_a (\rho v_a), \quad (16)$$

$$\partial_t m_b = \partial_a (u_a m_b + p \delta_{ab}), \quad (17)$$

$$\partial_t E = \partial_a (u_a E + u_a p). \quad (18)$$

The numerical method we used is as follows, based on a function $\text{Flux}_a(\mathbf{U}\mathbf{0})$ which calculates the fluxes across the cell surfaces using a Riemann solver. $\text{Flux}_a(\mathbf{U}\mathbf{0})$ is defined as follows. First, $\mathbf{V}\mathbf{0}$ are the primitive variables calculated from $\mathbf{U}\mathbf{0}$:

$$\mathbf{V}\mathbf{0} = \mathbf{V}(\mathbf{U}\mathbf{0}). \quad (19)$$

The interpolated primitive variables $\mathbf{V}\mathbf{L}$ and $\mathbf{V}\mathbf{R}$ are

$$(\mathbf{V}\mathbf{R}[\mathbf{i} - \frac{1}{2}\mathbf{e}_a], \mathbf{V}\mathbf{L}[\mathbf{i} + \frac{1}{2}\mathbf{e}_a]) =$$

$$\text{Interpolate}(\mathbf{V0}[\mathbf{i} - \mathbf{e}_a], \mathbf{V0}[\mathbf{i}], \mathbf{V0}[\mathbf{i} + \mathbf{e}_a]), \quad (20)$$

where we use piecewise linear interpolation with MINBEE flux limiter [31, 30]:

$$\begin{aligned} \text{Interpolate}(y0, y1, y2) &= (y1 - \frac{1}{2}dy, y1 + \frac{1}{2}dy) \quad \text{where} \\ dy01 &= y1 - y0 \\ dy12 &= y2 - y1 \\ dy &= \begin{cases} 0 & \text{if } dy01 \cdot dy12 < 0 \\ dy01 & \text{if } |dy01| < |dy12| \\ dy12 & \text{otherwise} \end{cases} . \end{aligned} \quad (21)$$

Then, fluxes across the boundaries are defined using the HLLC Riemann solver [32].

$$\mathbf{F}_a[\mathbf{i} + \frac{1}{2}\mathbf{e}_a] = \text{HLLC}_a(\mathbf{VL}[\mathbf{i} + \frac{1}{2}\mathbf{e}_a], \mathbf{VR}[\mathbf{i} + \frac{1}{2}\mathbf{e}_a]). \quad (22)$$

This is the flux defined by $\text{Flux}_a(\mathbf{U0})$. Then, linear addition of flux to conserved variable $\text{AddFlux}(\Delta t, \mathbf{F}_a, \mathbf{U})$ is defined by

$$\begin{aligned} \mathbf{U2} &= \text{AddFlux}(\Delta t, \mathbf{F}_a, \mathbf{U1}) \\ \Leftrightarrow \mathbf{U2}[\mathbf{i}] &= \mathbf{U1}[\mathbf{i}] + \sum_a \frac{\Delta t}{\Delta r_a} (\mathbf{F}_a[\mathbf{i} - \frac{1}{2}\mathbf{e}_a] - \mathbf{F}_a[\mathbf{i} + \frac{1}{2}\mathbf{e}_a]), \end{aligned} \quad (23)$$

where Δr_a is the mesh-size along the a -axis. Using these notations, we construct the second-order time marching as follows, where Δt is the time step determined by the CFL-condition:

$$\mathbf{F0}_a = \text{Flux}_a(\mathbf{U0}) \quad (24)$$

$$\mathbf{U1} = \text{AddFlux}(\frac{1}{2}\Delta t, \mathbf{F0}_a, \mathbf{U0}) \quad (25)$$

$$\mathbf{F1}_a = \text{Flux}_a(\mathbf{U1}) \quad (26)$$

$$\mathbf{U2} = \text{AddFlux}(\Delta t, \mathbf{F1}_a, \mathbf{U0}) \quad (27)$$

$\mathbf{U2}$ is the set of conserved variables for the next generation.

Notice how we rely on human mind flexibility when we convey the algorithms in the forms like above. In languages like Fortran or C, we are often forced to decompose those expression into elemental expressions and the source codes tend to become longer. In Haskell, we can express these ideas in well-defined machine readable forms while keeping the compactness and flexibility as in above.

We declare both the primitive variables Eq. (13) and conserved variables Eq. (14) as instances of the type class `Hydrable`, the set of variables large enough for calculating any other hydrodynamic variables. We used the general form by default, and `bind` either the primitive or conserved variables when we need the specific form. By doing so requisite minimum number of conversion code between primitive and conserved variables are generated.

When we defined the MINBEE interpolation for a triplet of real numbers Eq. (21) and then applied it to primitive variables Eq. (20), we implicitly extended a function on real numbers to function on set of real numbers. In Haskell, we can define how any such generalized function application over the set of hydrodynamic variables should behave, just by making it an instance of `Applicative` type class.

ID	config	(1)	(2)	lines	subKernel	memory
<i>Izanagi</i>	32×32	D	D	13128	7	$52 \times N$
<i>Izanami</i>	448×256	D	D	13128	7	$52 \times N$
<i>Iwatsuchibiko</i>	448×256	M	D	17494	12	$68 \times N$
<i>Shinatsuhiko</i>	448×256	D	M	3010	11	$68 \times N$
<i>Hayaakitsuhome</i>	448×256	M	M	3462	15	$84 \times N$

ID	score (SP)	score (DP)
<i>Izanagi</i>	1.551 ± 0.0005	1.138 ± 0.000
<i>Izanami</i>	5.838 ± 0.004	3.091 ± 0.002
<i>Iwatsuchibiko</i>	5.015 ± 0.002	2.491 ± 0.001
<i>Shinatsuhiko</i>	42.682 ± 0.083	19.831 ± 0.021
<i>Hayaakitsuhome</i>	34.100 ± 0.110	15.632 ± 0.024

Table 5. The codes annotated by hand and their performances. First four columns are the ID of the individuals, the CUDA kernel execution configuration, and the two choices of annotation — whether to **Manifest** or **Delay** (1) the result of spatial interpolation (2) the result of the Riemann solver. Next three columns are the properties of the generated codes as results of these choices made. They are namely the size of the code (number of lines), the number of subKernels in the code, the memory consumption in proportion to fluid cell number N . The last two columns are the speed of the generated codes for single precision (SP) and double precision (DP). The speed of the codes are measured by Mcups (10^6 cell update per second).

When we calculate the space-derivatives of the fluxes in Eq. (23), the component of the flux we access (index a in \mathbf{F}_a) and the direction in which we differentiate (indices a in $[\mathbf{i} - \frac{1}{2}\mathbf{e}_a]$ and $[\mathbf{i} + \frac{1}{2}\mathbf{e}_a]$) should match. Although the flux \mathbf{F} and the spatial array indices \mathbf{i} have very different types, Haskell’s type inference guarantees that they are both tensors of the same dimensions, and we can access both of them by the common tensor index a . And we can sum over a , because tensors are **Foldable** and their components are **Additive**. Tensors are **Traversable** as mentioned before, and any type constructors that are **Traversable** are also **Foldable**.

4.2. Annotating By Hand

Before we start the automated tuning experiment, we generate several individuals by hand. The initial individual *Izanagi* is the one with the least number of **Manifest** nodes as possible. *Izanami* is the same individual with the CUDA execution configuration suggested by the CUDA occupancy calculator. Based on it, we add several **Manifest** annotation and create new individuals (c.f. Table 5). Manual annotations are not blind-search process; each annotation has clear motivation such as “let us store the result of the Riemann solvers because it is computationally heavy”, “let us store the result of interpolations because it moves a lot of data,” etc. For example, the sample code in Table 6 shows the implementation of the piecewise linear interpolation with the MINBEE

The interpolation code for *Izanami*:

```
interpolateSingle order x0 x1 x2 x3
| order == 1 = do
  return (x1, x2)
| order == 2 = do
  d01 <- bind $ x1-x0
  d12 <- bind $ x2-x1
  d23 <- bind $ x3-x2
  let absmaller a b = select ((a*b) 'le' 0) 0 $
                          select (abs a 'lt' abs b) a b
  d1 <- bind $ absmaller d01 d12
  d2 <- bind $ absmaller d12 d23
  l <- bind $ x1 + d1/2
  r <- bind $ x2 - d2/2
  return (l,r)
```

For *Iwatsuchibiko*, the last line is modified as follows:

```
return (Anot.add Alloc.Manifest <?> l, Anot.add Alloc.Manifest <?> r)
```

Table 6. An annotation made in Paraiso source code that causes the results of the interpolations to be stored on memory and reused.

flux limiter, Eq. (21) in Paraiso, and how to annotate the return values of the limiter as `Manifest`.

We use *Izanami* as the base line of the benchmark, and use *Izanagi* as the initial individual of some experiment to see if the automated tuning can find out the optimal CUDA execution configuration by itself.

The codes are benchmarked on TSUBAME 2.0 cluster at Tokyo Institute of Technology. Each individual was benchmarked on a TSUBAME node with two Intel Xeon X5670 CPU(2.93GHz, 6 Cores \times HT = 12 processors) and three M2050 GPU(1.15GHz 14MP \times 32Cores/MP=448Cores).

The abstraction power of `Builder Monad` lets us change the code drastically with little modification. For example, Paraiso source code of *Shinatsuhiko* and *Izanami* differs by just one line of annotation. This introduces the 16 bits of difference in their genome, causing *Shinatsuhiko* generate a code that has 1/3 lines, which contains four more subroutines, consume 1.31 times more memory and is 6.42 times faster.

4.3. Automated Tuning

Next, we performed several automated tuning experiments c.f. Table 7.

To distinguish the contribution of the three methods to generate new individuals, we also performed automated tuning experiments with either crossover or triangulation turned off. Table 8 shows the initial possibility of the master node attempting each

RunID	prec.	initial score	wct	best ID/total	high score
GA-1	DP	1.138 ± 0.000	3870	20756 / 20885	14.158 ± 0.002
GA-S1	DP	1.138 ± 0.000	4120	33958 / 34328	16.247 ± 0.002
GA-DE	DP	19.253 ± 0.044	7928	41250 / 41386	31.015 ± 0.032
GA-D	DP	19.253 ± 0.044	8770	59841 / 68138	34.968 ± 0.043
GA-4	DP	19.253 ± 0.044	5811	39991 / 40262	35.303 ± 0.035
GA-F	SP	42.682 ± 0.083	2740	23019 / 23062	53.300 ± 0.078
GA-F2	SP	42.682 ± 0.083	4811	22242 / 24887	53.656 ± 0.078
GA-3D	SP	24.638 ± 0.001	5702	38146 / 39200	45.443 ± 0.116

Table 7. The statistics of auto-tuning experiments. The columns are RunID, precision, the score of initial individual, the wall-clock time for the experiment (in minutes), the ID of the best individual and the number of individuals generated, the high score (in Mcups). Experiments GA-1 and GA-S1 started with *Izanagi*, others started with *Shinatsuhiko*. GA-3D started with *Shinatsuhiko*, and solved 3D problems.

	mutation	crossover	triangulation
GB-333	1/3	1/3	1/3
GB-370	1/3	2/3	0
GB-307	1/3	0	2/3

Table 8. The probability of the master node attempting each method of birth in experiment series GB-*

RunID	prec.	initial score	best ID/total	high score
GB-333-0	DP	19.253 ± 0.044	35294 / 40014	25.343 ± 0.028
GB-333-1	DP	19.253 ± 0.044	40256 / 40031	26.402 ± 0.023
GB-333-2	DP	19.253 ± 0.044	39206 / 40033	32.758 ± 0.006
GB-370-0	DP	19.253 ± 0.044	36942 / 39994	24.698 ± 0.045
GB-370-1	DP	19.253 ± 0.044	37468 / 40045	28.339 ± 0.042
GB-370-2	DP	19.253 ± 0.044	39719 / 40032	31.669 ± 0.039
GB-307-0	DP	19.253 ± 0.044	30320 / 40018	21.744 ± 0.035
GB-307-1	DP	19.253 ± 0.044	39358 / 40002	26.349 ± 0.026
GB-307-2	DP	19.253 ± 0.044	38107 / 40053	27.412 ± 0.005

Table 9. The statistics of GB-* experiment series. The columns are RunID, precision, the score of initial individual, the ID of the best individual and the number of individuals generated, the high score (in Mcups). Experiments started with *Shinatsuhiko*. The nine experiments were performed in parallel, and took 92252 minutes of wall-clock time.

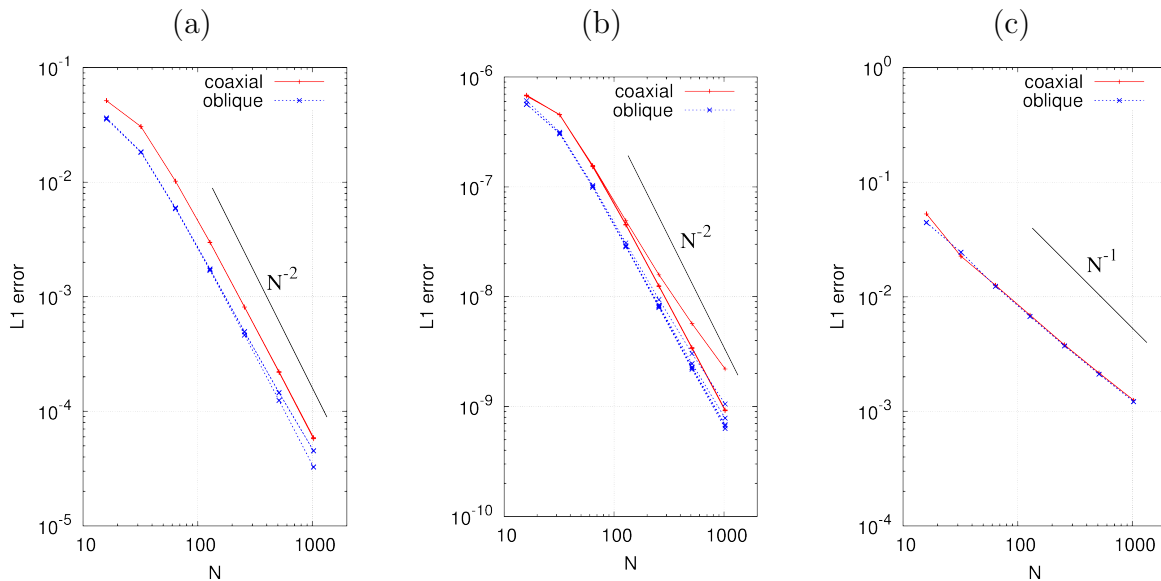


Figure 10. Convergence tests of the norm of the L_1 error vector of density field for (a) entropy waves, (b) sound waves and (c) shock-tube problem.

method of birth. Note that the actual frequencies of crossover and triangulation are smaller than these value because the master may default to mutation. Table 9 shows the result of experiments. The resolutions were 1024^2 for GA-1 and GA-S1, problems, 100^3 for GA-3D problems and 512^2 for other GA-* series. The resolutions were 512^2 in GB-* series.

The automated tuning system can generate and benchmark approximately 10'000 individuals per day. 20 – 100 workers were running at the same time. It takes a few days to tune up *Izanami* to speed comparable to *Shinatsuhiko*, or speed up *Shinatsuhiko* by another factor of 2. The best speed obtained was 35.3Mcups for double precision, and 53.7Mcups for single precision. Our automated tuning experiments on 3D solvers mark 42.4Mcups SP. These are competitive performances to hand-tuned codes for single GPUs; e.g. Schive et. al. [33] reports 30Mcups per C2050 card (single precision, note that their code is 3D. Asunción et.al. [34] reports 6.8Mcups per GTX580 card (single precision, 2D).

Fig. 10 shows the result of convergence tests for individuals *GA-1.20756*, *GA-4.33991*, *GA-D.59841*, *GA-DE.41250*, *GA-S1.33958*, *Izanami* and *Shinatsuhiko*. The resolution N is varied from 16^2 to 1024^2 . The codes are tested for entropy wave propagation, sound wave propagation and Sod's shock-tube problem. The detail of test initial conditions are as follows. For all tests, numerically solved domains are $(0 < x < 1, 0 < y < 1)$, out of which the analytic solutions are continuously substituted as boundary conditions. The system was numerically developed until $t = 1$ for entropy wave and sound wave problems, and $t = 0.125$ for shock tube problem, and then the numerical solutions were compared to analytic solutions using the norm of L_1 error vector.

The initial conditions are, for entropy wave problem:

$$\left\{ \begin{array}{l} \rho(x, y) = 2 + \sin(2\pi x), \\ v_x(x, y) = 1, \\ v_y(x, y) = 0, \\ p(x, y) = 1, \end{array} \right. \quad (28)$$

for sound wave problem:

$$\left\{ \begin{array}{l} \rho(x, y) = \gamma(1 + A \sin(2\pi x)) \\ v_x(x, y) = A \sin(2\pi x), \\ v_y(x, y) = 0, \\ p(x, y) = 1 + \gamma A \sin(2\pi x), \end{array} \right. \quad (29)$$

where the amplitude $A = 10^{-5}$, and for Sod's shock-tube problem:

$$x < 0.5 \left\{ \begin{array}{l} \rho(x, y) = 1, \\ v_x(x, y) = 0, \\ v_y(x, y) = 0, \\ p(x, y) = 1, \end{array} \right. \quad (30)$$

$$x > 0.5 \left\{ \begin{array}{l} \rho(x, y) = 0.125, \\ v_x(x, y) = 0, \\ v_y(x, y) = 0, \\ p(x, y) = 0.1. \end{array} \right. \quad (31)$$

While the ‘‘coaxial’’ tests used the above initial conditions as they are, the ‘‘oblique’’ tests used the initial conditions rotated about $(x, y) = (0.5, 0.5)$ for 60° .

5. Analysis on the Automated Tuning Experiments

5.1. Overview of The Simulated Evolution and Analyses

The functions of score against evolution progress exhibit self-similar structure of repeated cliff and plateau. For example, see the evolution history of experiment GA-D illustrated in Fig. 11 and its two enlarged views Fig. 12 and Fig. 13, with the family tree of the best individual superimposed. The evolution of the high scores in the experiments are shown in Fig. 14.

To design more efficient auto-tuning strategies, we investigate what have happened and which part of the evolution contributed to create better individuals in our automated tuning experiments. In section 5.2, we measure the contributions from three different tuning items. In section 5.3, we classify the individuals by their aspects such as their method of birth, their distance to the champion in the family tree, and their fitness relative to their parents. In section 5.4 we study how these classes contribute to the evolution by performing correlation analyses among these classes. In section 5.5, we study how the method of birth of parents affect their children. In section 5.6 we summarize and conclude the analyses.

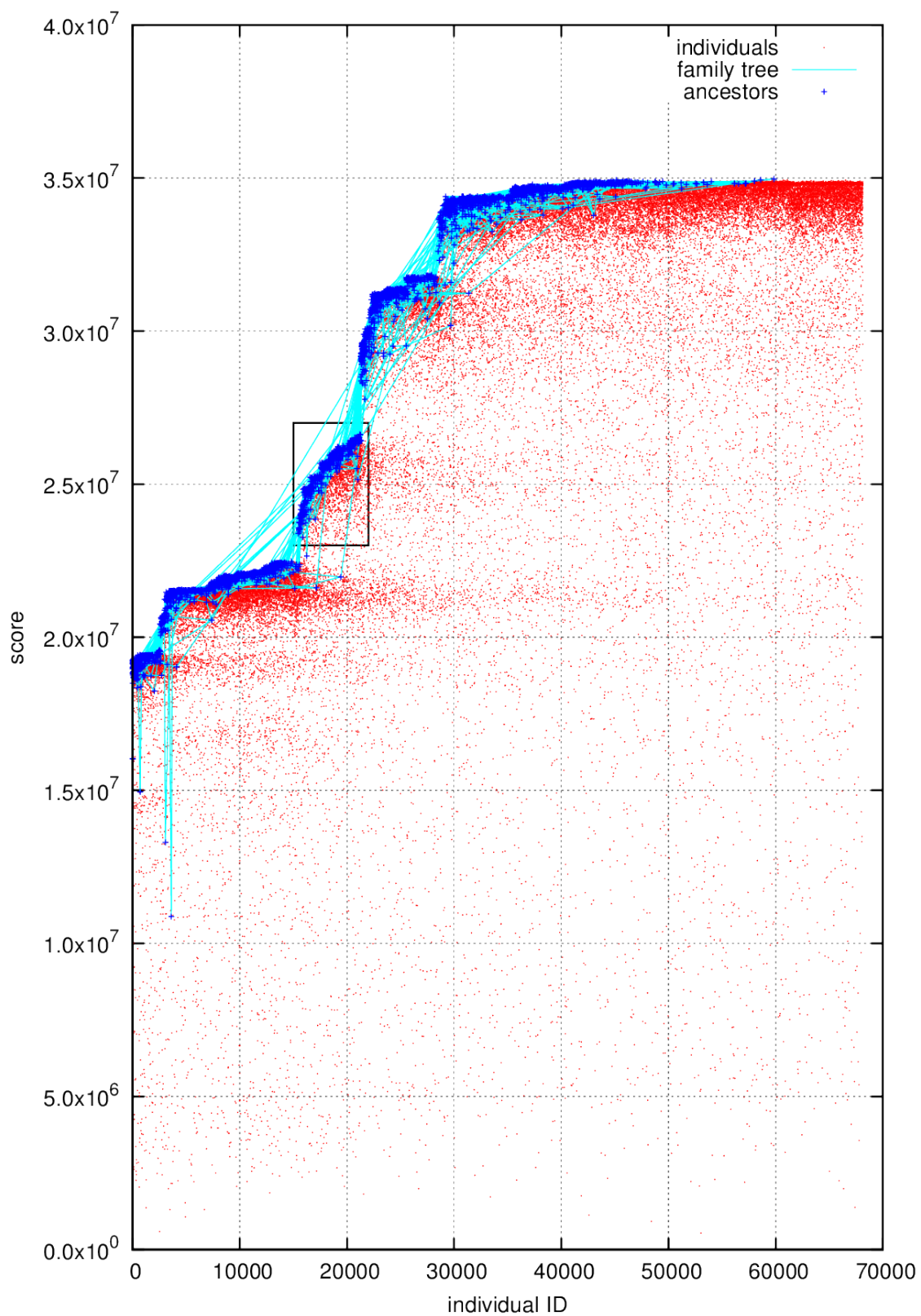


Figure 11. The ID and the scores (in cups) of all the individuals generated in automated tuning experiment GA-D. The individual with the highest score as well as its ancestors are marked by crosses, and each of them is connected to its parents with lines.

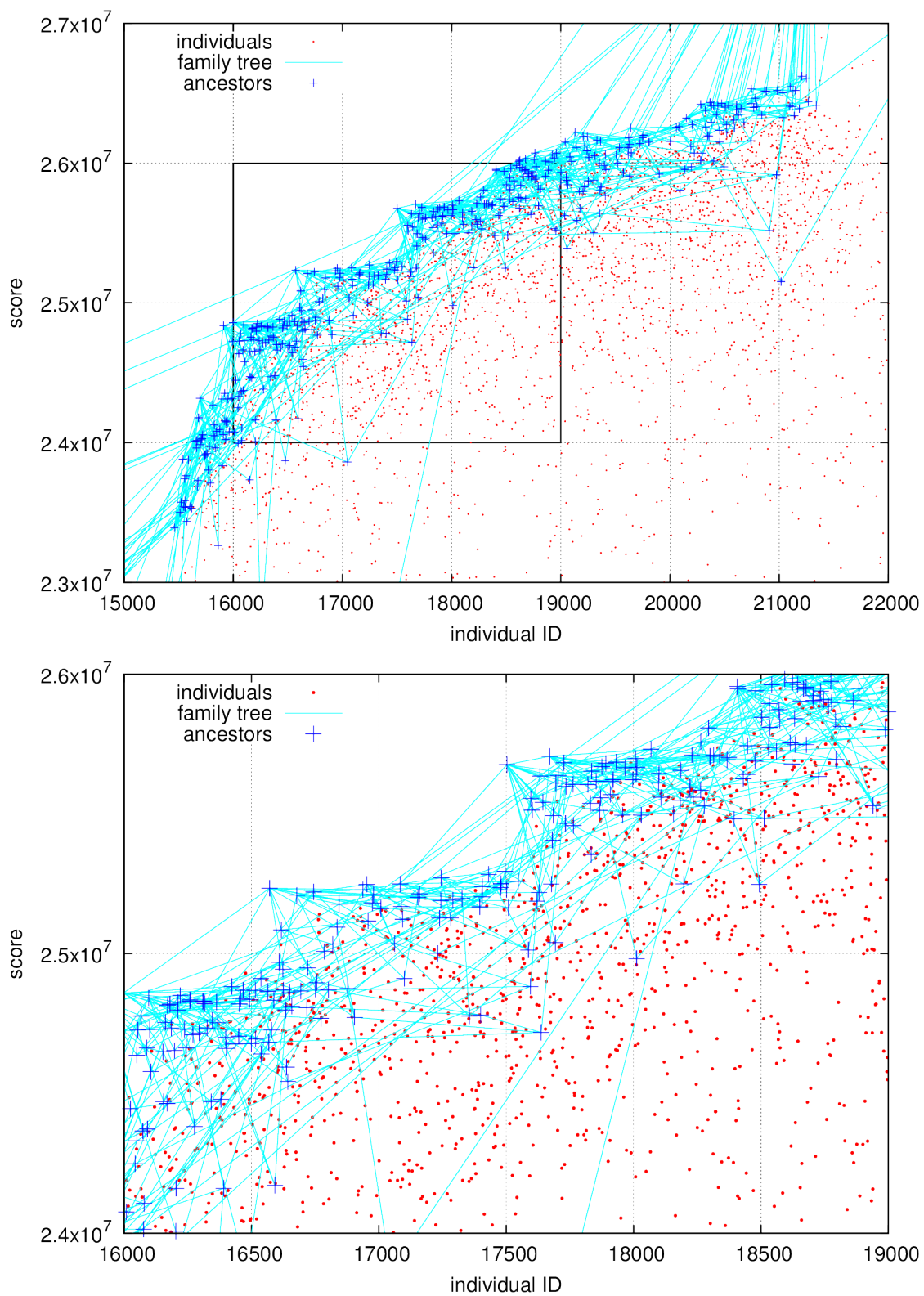


Figure 12. Two enlarged views of Fig. 11

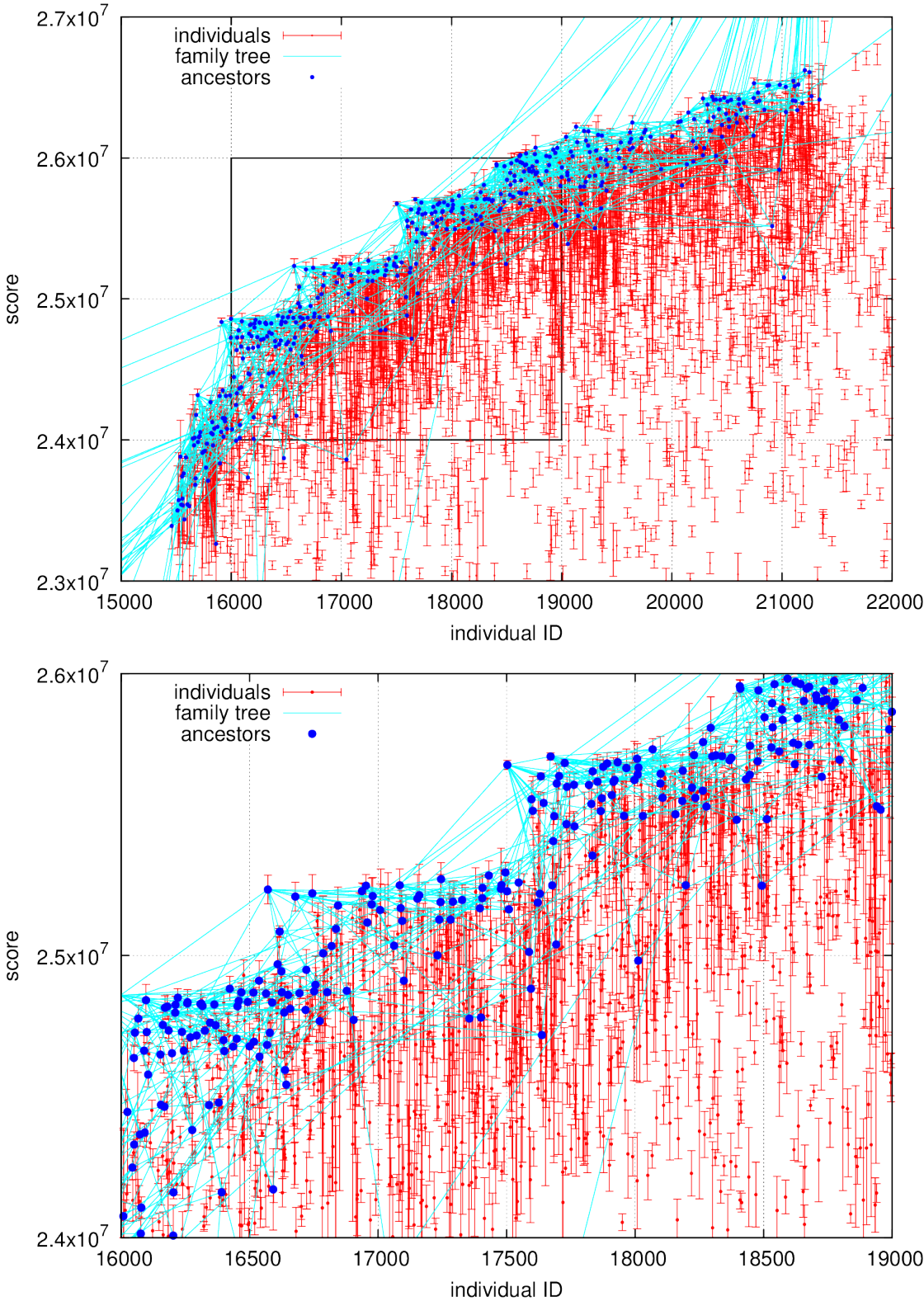


Figure 13. Two enlarged views of Fig. 11 showing $\mu(I)$ and $\sigma(I)$ as functions of I .

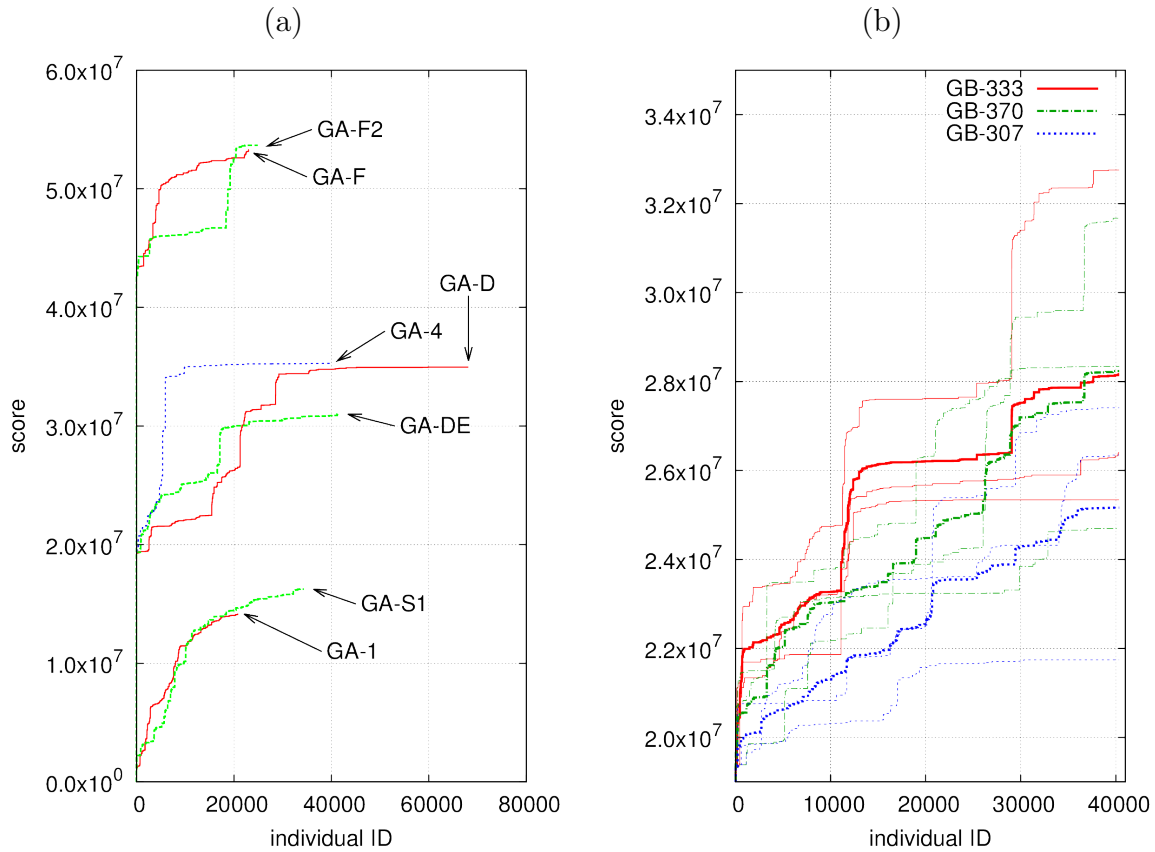


Figure 14. The evolution of the high score (in cups) as functions of ID in (a) experiments GA-* and (b) experiments GB-*. The three thick curves are the average of the GB-333-*, GB-370-* and GB-307-*, respectively. The average of GB-370-* was always higher than that of GB-307-*, and the average of GB-333-* was always higher than that of GB-370-* for the 89% of the time.

5.2. Contributions of The Three Genome Parts

We assign the symbols to genome parts with different functions as follows: (C): the CUDA kernel execution configuration, (M): which data to store on the memory (to make them **Manifest**), and (S): when to synchronize the computation. We first investigate how these three components contributed to the score by component-wise artificial crossover between the initial individual and the best scoring individual (Table 10). In the case of *GA-S1.33958*, introducing improvement only in C, M, S part increase the score by 14%, 30%, and 0%, respectively. In the case of *GA-4.33991*, the increase are 0%, 85%, 0%. Both cases exhibit synergy effect. Introducing several modifications simultaneously have more effect than the sum of the separate effects, they multiply. So addition in log-space explains 98% and 88% of the progress for *GA-S1.33958* and *GA-4.33991*, respectively, but the score of the final individuals are still slightly higher than predicted.

Removing only one of C,M,S part from *GA-4.33991* decreases the score by 16%,

ID	C	M	S	score(Mcups)	relative score	logscale
<i>Izanagi</i>	0	0	0	1.137 ± 0.003	0.000 ± 0.000	0.000 ± 0.001
	0	0	1	1.122 ± 0.000	-0.001 ± 0.000	-0.005 ± 0.000
	0	1	0	5.400 ± 0.006	0.300 ± 0.000	0.599 ± 0.000
	0	1	1	5.300 ± 0.006	0.293 ± 0.000	0.591 ± 0.000
	1	0	0	3.073 ± 0.002	0.136 ± 0.000	0.382 ± 0.000
	1	0	1	2.946 ± 0.000	0.127 ± 0.000	0.366 ± 0.000
	1	1	0	15.829 ± 0.027	1.033 ± 0.002	1.012 ± 0.001
<i>GA-S1.33958</i>	1	1	1	15.354 ± 0.020	1.000 ± 0.001	1.000 ± 0.001
<i>Shinatsuhiko</i>	0	0	0	19.808 ± 0.033	0.000 ± 0.002	0.000 ± 0.003
	0	0	1	19.817 ± 0.030	0.001 ± 0.002	0.001 ± 0.003
	0	1	0	32.821 ± 0.058	0.848 ± 0.004	0.880 ± 0.003
	0	1	1	32.694 ± 0.057	0.839 ± 0.004	0.873 ± 0.003
	1	0	0	19.773 ± 0.050	-0.002 ± 0.003	-0.003 ± 0.004
	1	0	1	19.859 ± 0.058	0.003 ± 0.004	0.005 ± 0.005
	1	1	0	32.994 ± 0.273	0.859 ± 0.018	0.889 ± 0.014
<i>GA-4.33991</i>	1	1	1	35.160 ± 0.082	1.000 ± 0.005	1.000 ± 0.004

Table 10. The score of the individuals created by artificial crossover between the initial individual I_0 and the best scoring individual I_\top . The second to fourth columns indicate which component was taken from which individual. Columns C,M,S correspond to CUDA kernel execution configuration, Manifest/Delay choice, synchronization timing, respectively. For each individual I the fifth column shows $\mu(I) \pm \sigma(I)$, the sixth column shows $\frac{\mu(I)}{\mu(I_\top) - \mu(I_0)} \pm \frac{\sigma(I)}{\mu(I_\top) - \mu(I_0)}$, and the seventh column shows $\frac{\log \mu(I) - \log \mu(I_0)}{\log \mu(I_\top) - \log \mu(I_0)} \pm \frac{\sigma(I)}{(\log \mu(I_\top) - \log \mu(I_0))\mu(I)}$.

100%, and 14%, respectively. Removing C,M,S part from *GA-S1.33958* decreases the score by 71%, 87%, and -3% , respectively. Again we see the synergy effect, except that *GA-S1.33958* were faster if S part were removed.

We conclude that the Manifest/Delayed trade-off plays the central part in improving the score. Fixing the Manifest/Delayed nodes, determines the decomposition of the data-flow graph. Then tuning the synchronization timing and CUDA kernel execution configuration help further improve the score.

5.3. Classifications of Individuals

To measure how each individual I contributed in generating one of the best individuals, we define contribution distance $d(I)$, and classify the individuals to those who contributed to the evolution and those who didn't. To begin with, let $\mathbb{P}(I)$ be the set of individual I 's parents. (we use p for probability.) For individual I born by mutation, crossover, and triangulation, the size of the parent set $n(\mathbb{P}(I))$ is 1,2, and 3,

respectively.

We define $d(I)$ as follows:

- $d(I_{\top}) = 0$ where I_{\top} is the individual whose $\mu(I)$ was the largest in the history.
- $d(I) = 0$ if $\mu(I) > \mu(I_{\top}) - \sigma(I_{\top})$.
- $d(I) = 0$ if one of I 's children I_c satisfies $d(I_c) = 0$.
- $d(I) = 1 + \min\{d(I_{\mathbb{P}}) | I_{\mathbb{P}} \in \mathbb{P}(I)\}$ otherwise.

We say that I is one of the best individuals if $\mu(I) > \mu(I_{\top}) - \sigma(I_{\top})$. For them, and their ancestors, $d(I) = 0$. For other individuals $d(I)$ is the graph theoretical distance from the family trees of the best individuals. Table A1 - A7 shows the distributions of $d(I)$ for individuals born of mutation, crossover, and triangulation.

Next, we compare the fitness of the children with their parents. We classify the individuals into four ranks, namely $[\ll]$, $[\leq]$, $[\simeq]$, and $[\gg]$, based upon comparison of their scores with parents' scores.

- $I \in [\ll]$ if $\forall I_{\mathbb{P}} \in \mathbb{P}(I) : \mu(I) < \mu(I_{\mathbb{P}}) - \sigma(I, I_{\mathbb{P}})$,
- $I \in [\gg]$ if $\forall I_{\mathbb{P}} \in \mathbb{P}(I) : \mu(I) > \mu(I_{\mathbb{P}}) + \sigma(I, I_{\mathbb{P}})$,
- $I \in [\simeq]$ if $|\mu(I) - \mu(I_{\mathbb{P}_1})| < \sigma(I, I_{\mathbb{P}_1})$ where $I_{\mathbb{P}_1}$ is the member of $\mathbb{P}(I)$ with the largest μ , and
- $I \in [\leq]$ otherwise,

where $\sigma(I, I_{\mathbb{P}}) \equiv (\sigma(I)^2 + \sigma(I_{\mathbb{P}})^2)^{0.5}$.

$[\gg]$ are children significantly faster than any of their parents; $[\simeq]$ are children whose scores are comparable to their fastest parents; $[\ll]$ are children significantly slower than any of their parents; and $[\leq]$ are children significantly slower than their best parent but not significantly slower than their slowest parents. Note that children of rank $[\leq]$ are never born by mutations since there is only one parent. Table A8 - A14 shows the classifications for experiments.

5.4. Chi-squared Tests of Correlations between Classes

To study which set of individuals are contributing to produce best species, we perform Pearson's chi-squared test on pairs of predicates on individuals; see Table A15 and A16. We use 10^{-3} significance, or $X^2 > 10.83$ unless otherwise mentioned. Our observations are as follows:

- (row 1.) Significant negative correlations are detected between being born of mutation ($n(\mathbb{P}(I)) = 1$) and being $d(I) = 0$ for all experiments.
- (row 2.) Significant positive correlations are detected between being born of crossover ($n(\mathbb{P}(I)) = 2$) and being $d(I) = 0$ for all experiments but GA-S1.
- (row 3.) Significant positive correlations are detected between being born of triangulation ($n(\mathbb{P}(I)) = 3$) and being $d(I) = 0$ for all experiments.

- (row 4, 5.) Significant positive correlations are detected between being ($I \in [\gg]$) and being $d(I) = 0$, and also between being ($I \in [\simeq]$) and being $d(I) = 0$ for all experiments.
- (row 6.) Being ($I \in [\leq]$) and being $d(I) = 0$ are negatively correlated for all experiments, but out of 10 experiments only 4 are 10^{-3} significant.
- (row 7.) Significant negative correlations are detected between being ($I \in [\ll]$) and being $d(I) = 0$ for all experiments.
- (row 8, 9.) Within the population born of either crossover or triangulation, being born of triangulation ($n(\mathbb{P}(I)) = 3$) and being $d(I) = 0$ are still positively correlated for all experiments, but significant experiments are 7 out of 10.
- (row 10, 11.) Within the elite population $\mathbb{E} \equiv \{I | n(\mathbb{P}(I)) \geq 2\} \cap ([\gg] \cup [\simeq])$, being ($I \in [\gg]$) and being $n(\mathbb{P}(I)) = 2$ are significantly and positively correlated.
- (row 12-15.) Within the family tree of the champions $d(I) = 0$, a subset of experiments shows that the pairs ($n(\mathbb{P}(I)) = 2, I \in [\gg]$) and ($n(\mathbb{P}(I)) = 3, I \in [\simeq]$) are positively correlated, and that the pairs ($n(\mathbb{P}(I)) = 2, I \in [\simeq]$) and ($n(\mathbb{P}(I)) = 3, I \in [\gg]$) are positively correlated. The number of significant examples are 7, 5, 2, and 7 out of 10, respectively, and no significant opposite correlation are observed.
- (row 16, 17.) Although 7 is considered to be a lucky number and 13 an unlucky number in Western culture, there is no correlation between having 7 at the lowest digit and being $d(I) = 0$, nor having 13 as the two lowest digits and being $d(I) \neq 0$. These are control experiments.

5.5. Correlation along the Family Line

Next, we analyze the correlation along the family line by interpreting the family tree as Markov processes (c.f. Table 11). For each individual I such that $d(I) = 0$, we trace back its family tree in all possible ways for n steps and obtain an n -letter word. For example, “312” means that I is born of crossover, and one of its parent was born of mutation from an individual who was born of triangulation. With such bag of words obtained, we investigate how the last letter of a word is correlated with letters in front of them.

The second columns show X^2 for null hypothesis “The bag of words is a 0th order Markov chain,” i.e. in the two-letter words the second letter is not correlated to the first. Formally written, the null hypothesis is:

$$p(ab) = p(a)p(b), \tag{32}$$

where a, b, c, \dots denote characters and ab, abc, \dots denote words.

The third columns show X^2 for null hypothesis “The bag of words is a 0th order Markov chain,” i.e. the probability of the occurrences of the letters depend only on their immediate predecessors and the distribution of three-letter words can be determined

RunID	0th order	1st order	2 → 2	3 → 3	22 → 2	33 → 3
GA-1	2263.22	266.28	⊖118.86	⊕1655.46	⊕32.54	⊕71.54
GA-S1	1387.93	70.51	⊖23.98	⊕1075.96	⊖5.19	⊕7.84
GA-DE	546.42	43.31	⊕3.34	⊕427.88	⊖9.85	⊕3.68
GA-D	1038.15	88.20	⊖42.78	⊕811.09	⊕3.90	⊕1.34
GA-4	755.63	39.91	⊖7.98	⊕580.33	⊖2.09	⊖2.60
GA-F	422.08	22.24	⊖2.07	⊕333.57	⊕0.96	⊖0.25
GA-F2	490.90	86.34	⊖23.63	⊕381.72	⊕16.29	⊕6.09
GB-333-0	666.18	47.52	⊖12.34	⊕511.62	⊕1.36	⊖2.52
GB-333-1	930.33	25.26	⊖48.06	⊕727.01	⊖0.86	⊖0.90
GB-333-2	1208.20	68.11	⊖39.34	⊕937.37	⊕0.34	⊖7.59

Table 11. Chi-squared test of the family tree being lower-order Markov processes. The each column of the table shows the X^2 statistics of the null hypothesis the family tree being a n -th order Markov process and having no longer correlation.

from the distribution of two-letter words. Formally written, the null hypothesis is:

$$p(abc) = \frac{p(ab) p(bc)}{p(b)}. \quad (33)$$

Table 11 shows the result of the Markov chain analysis. Note that, the degree of freedom k for 0th-order and 1st-order Markov chains are 4 and 16, respectively, and the chi-squared values for 10^{-3} significance are $X^2 > 18.47$ and $X^2 > 37.70$, respectively. From the table, we can deny the 0th-order Markov chain model for all of the experiments, and deny the 1st-order Markov chain model for 8 out of the 10 experiments. We also studied whether an occurrence of a character is correlated to its prefix word. “3” was significantly likely to be followed by another “3” in all of the experiments, while “2” was significantly unlikely to be followed by another “2” in 6 out of 10 experiments. On the other hand, three consecutive occurrences of the same letter was not significant at least in 8 out of 10 experiments.

5.6. Summary of The Analyses

Mutation is not efficient in directly producing individuals with good scores. Nevertheless mutations are indispensable part of the evolution because it is the only way that introduces new genomes to the genome pools and that have chance of finding new improvements.

Triangulations and crossover are two different methods to combine independently-found improvements, and are efficient in directly producing good individuals. Triangulations are relatively more efficient in producing $d(I) = 0$ individuals. However, crossover is relatively good at making large jumps that belongs to $[\gg]$. Triangulations are working in another way; the statistics indicate that one triangulation are likely to be followed by another triangulation in a family tree, and the sequence of Triangulations

work to accumulate minor improvements that belongs to $[\simeq]$ to make a larger one. Fig. 14 — although the number of samples are too few to make a statistically significant statement — suggests that having both mode of combiner is better than having only one.

The main source of performance improvement was the change in memory layout and subroutine re-organization caused by making different Manifest/Delayed trade-offs. Tuning the synchronization timing and CUDA kernel execution configuration provided additional improvements.

The case of *GA-S1.33958* is an evidence of the current genetic algorithm not finding the optimal individual. Random mutations tend to increase the genome entropy even under the selection pressure. Adding the rule-based mutations such as “remove all synchronization,” which are improbable under random mutations, may contribute to further optimization.

6. Conclusion and Discussion

We have designed and implemented Paraiso, a domain specific language for describing explicit solvers of partial differential equations, embedded in Haskell. Using the typelevel-tensor and algebraic type classes, we can explain our algorithms with simplicity of mathematical equations. Then the algorithm is translated to OpenMP code or CUDA code. The generated code can be optimized both by applying annotations by hand, and by automated tuning based on a genetic algorithm. Although we present just one example here — a second order Euler equations solver — the front end of Paraiso with typelevel-tensor and **Builder Monad** readily accept various other algorithms. The code generation and automated tuning can revolutionize the way we invent, implement and optimize various partial differential equation solvers.

The website of Paraiso is <http://www.paraiso-lang.org/wiki/>, where you can find codes, documentations, slides and videos.

Making more efficient searches for fast individuals is an important future extension of Paraiso. One way is to use machine learning, for example to make suggestions for genomes to introduce, or to predict the scores of the individuals before benchmarking them. Another approach is careful selection of the tuning items, importance of them given either by hand or by inference from the syntactic structure of Paraiso source code. The computing time invested in automated tuning is only justified if the optimized program is used repeatedly, or if optimized single-GPU program is used as a “core” of a multi-GPU program.

Making the automated tuning results more flexible and re-usable is another future challenge. For example, the size of the array e.g. $(N0, N1)$ in §2.2 for the two-dimensional OM, is fixed before native code generation under the current design of Paraiso. To change the size $N0$ or $N1$, the users need to re-run the code generation process. One solution is to improve the representation of the constant values in Paraiso, so that the users can set the values that are constant within a run but may vary

across different runs. Possible examples of such constants include the OM size and the parameters of the algorithm.

On the other hand, the change in the dimension of the OM e.g. to three; $(N0, N1, N2)$, or the change in the algorithm described by the Builder Monad will change the number of nodes in the OM data flow graph and the bits in the genome. Therefore, the automatically tuned genomes before the change become useless. The genome must be redesigned to perform more re-usable, general automated tunings.

Generating codes for distributed computers / distributed and accelerated computers is another important future extension of Paraiso. To this end, instead of generating MPI codes by ourselves, we plan to generate parallel languages such as X10 [35], Chapel [36], and XcalableMP [15], or domain specific languages for stencil computations such as Physis [5].

Finally, the potential users and developers of Paraiso are obstructed by the programming language Haskell, which is a very computer-science language and is far from being mainstream in the fields of simulation science and high-performance computing. This is a disadvantage of Paraiso compared to other embedded DSL approaches based on more popular syntax such as Python (e.g. [37].) We make two remarks on this.

On the one hand, we show in this paper that abstract concepts developed by computer scientists and found in Haskell, is useful and was almost necessary in implementing a DSL that consistently handles the translation from mathematical notations to evolutionary computation. We hope that such powerful DSLs appear in many different fields, with help of the findings in computer science. On the other hand, we want many other researchers to become developers and users of Paraiso without requiring much knowledge in computer science.

For promotion of such development and use of Paraiso, we plan to provide interfaces to the code generation and the tuning stages in Paraiso, in terms of strings or in lightweight markup languages, along with their specifications. Those will allow many other programming languages can access those stages, such as OM data-flow graphs, their annotations, and the genomes. Adding a simulation scientist friendly scripting language layer on top of Builder Monad is another future work, so that people not familiar with Haskell can access Paraiso. We also plan to publish a series of tutorials and example programs in the Paraiso website. Such collaborations are fundamental to the realization of the future works listed in this section and computer-assisted programming in many fields of simulation science.

Acknowledgments

The authors thank the anonymous referees for a number of suggestions that improved this paper. T.M. is supported by The Hakubi Center for Advanced Research. T.M. is also supported by Grants-in-Aid from the Ministry of Education, Culture, Sports, Science, and Technology (MEXT) of Japan, No. 24103506. The use of TSUBAME2.0

Grid Cluster in this project was supported by JST, CREST through its research program: “Highly Productive, High Performance Application Frameworks for Post Petascale Computing.”

Appendix A. supplementary data

$d(I)$	mutation	crossover	triangulation	total
0	1627(0.171)	1875(0.433)	3011(0.440)	6513(0.315)
1	4492(0.473)	1368(0.316)	2639(0.385)	8499(0.411)
2	2434(0.256)	944(0.218)	1129(0.165)	4507(0.218)
3	831(0.088)	141(0.033)	69(0.010)	1041(0.050)
4	104(0.011)	5(0.001)	2(0.000)	111(0.005)
5	6(0.001)	0(0.000)	0(0.000)	6(0.000)
6	1(0.000)	0(0.000)	0(0.000)	1(0.000)
sum	9495(1.000)	4333(1.000)	6850(1.000)	20678(1.000)

Table A1. Contribution distance analysis for experiment GA-1 : The numbers of individuals with specific $d(I)$ that is born of mutation, crossover, and triangulation. The last column shows the total numbers of individuals with specific $d(I)$. The decimal numbers inside the parentheses are the ratio of the number of individuals with specific $d(I)$ of specific birth, divided by total number of individuals of specific birth. Note that the grand total is slightly smaller than that in Table 7; this is because some worker nodes failed to write into DB.

$d(I)$	mutation	crossover	triangulation	total
0	1304(0.082)	915(0.106)	1411(0.145)	3631(0.106)
1	6136(0.386)	3601(0.416)	4696(0.481)	14433(0.421)
2	5461(0.344)	3211(0.371)	3161(0.324)	11833(0.345)
3	2392(0.151)	837(0.097)	470(0.048)	3699(0.108)
4	507(0.032)	79(0.009)	25(0.030)	611(0.018)
5	80(0.005)	7(0.001)	0(0.000)	87(0.003)
6	7(0.000)	0(0.000)	0(0.000)	7(0.000)
7	1(0.000)	0(0.000)	0(0.000)	1(0.000)
sum	15888(1.000)	8650(1.000)	9763(1.000)	34302(1.000)

Table A2. Contribution distance analysis for experiment GA-S1.

$d(I)$	mutation	crossover	triangulation	total
0	480(0.023)	430(0.047)	592(0.051)	1503(0.036)
1	10130(0.495)	4149(0.458)	6080(0.519)	20359(0.494)
2	6952(0.340)	3830(0.423)	4640(0.396)	15422(0.374)
3	2499(0.122)	622(0.069)	387(0.033)	3508(0.085)
4	385(0.019)	34(0.004)	12(0.001)	431(0.010)
5	21(0.001)	0(0.000)	0(0.000)	21(0.001)
6	4(0.000)	0(0.000)	0(0.000)	4(0.000)
7	1(0.000)	0(0.000)	0(0.000)	1(0.000)
sum	20472(1.000)	9065(1.000)	11711(1.000)	41249(1.000)

Table A3. Contribution distance analysis for experiment GA-DE.

$d(I)$	mutation	crossover	triangulation	total
0	785(0.023)	1099(0.071)	1680(0.087)	3565(0.052)
1	16113(0.482)	6208(0.403)	9699(0.503)	32020(0.470)
2	11510(0.344)	6946(0.451)	7490(0.389)	25946(0.381)
3	4509(0.135)	1139(0.074)	408(0.021)	6056(0.089)
4	472(0.014)	13(0.001)	1(0.000)	486(0.007)
5	21(0.001)	0(0.000)	0(0.000)	21(0.000)
6	2(0.000)	0(0.000)	0(0.000)	2(0.000)
sum	33412(1.000)	15405(1.000)	19278(1.000)	68096(1.000)

Table A4. Contribution distance analysis for experiment GA-D.

$d(I)$	mutation	crossover	triangulation	total
0	631(0.037)	730(0.066)	940(0.078)	2302(0.057)
1	7674(0.450)	5234(0.475)	6658(0.554)	19566(0.488)
2	6062(0.356)	4397(0.399)	4215(0.350)	14674(0.366)
3	2385(0.140)	644(0.058)	214(0.018)	3243(0.081)
4	291(0.017)	8(0.001)	0(0.000)	299(0.007)
5	9(0.001)	0(0.000)	0(0.000)	9(0.000)
sum	17052(1.000)	11013(1.000)	12027(1.000)	40093(1.000)

Table A5. Contribution distance analysis for experiment GA-4.

$d(I)$	mutation	crossover	triangulation	total
0	373(0.031)	329(0.068)	499(0.082)	1202(0.052)
1	6440(0.533)	2137(0.441)	3302(0.540)	11879(0.515)
2	3854(0.319)	2112(0.436)	2224(0.363)	8190(0.355)
3	1285(0.106)	262(0.054)	95(0.016)	1642(0.071)
4	137(0.011)	2(0.000)	0(0.000)	139(0.006)
5	4(0.000)	0(0.000)	0(0.000)	4(0.000)
sum	12093(1.000)	4842(1.000)	6120(1.000)	23056(1.000)

Table A6. Contribution distance analysis for experiment GA-F.

$d(I)$	mutation	crossover	triangulation	total
0	332(0.024)	314(0.076)	767(0.113)	1414(0.057)
1	7187(0.516)	1648(0.397)	3641(0.538)	12476(0.502)
2	4641(0.333)	1884(0.454)	2264(0.335)	8789(0.354)
3	1564(0.112)	295(0.071)	95(0.014)	1954(0.079)
4	190(0.014)	5(0.001)	0(0.000)	195(0.008)
5	21(0.002)	0(0.000)	0(0.000)	21(0.001)
sum	13935(1.000)	4146(1.000)	6767(1.000)	24849(1.000)

Table A7. Contribution distance analysis for experiment GA-F2.

mutation 9437(1.000)			crossover 4335(1.000)				triangulation 6834(1.000)			
[\ll]	[\simeq]	[\gg]	[\ll]	[\leq]	[\simeq]	[\gg]	[\ll]	[\leq]	[\simeq]	[\gg]
7468	935	1022	934	1228	824	1347	976	2161	2420	1293
(0.787	0.098	0.108)	(0.216	0.283	0.190	0.311)	(0.142	0.315	0.353	0.189)
202	516	856	77	392	517	889	20	573	1593	825
(0.021	0.054	0.090)	(0.018	0.090	0.119	0.205)	(0.003	0.084	0.233	0.120)
0.027	0.552	0.838	0.082	0.319	0.627	0.660	0.020	0.265	0.658	0.638

Table A8. Children relative fitness for Experiment GA-1: The individuals classified based upon how they were born and their score with respect to their parents. For each class, the first row shows the number of individuals of that class, and the third row shows the number of individuals of that class with $d(I) = 0$. The second and fourth rows are first and third row divided by the total number of individuals born in that way. The fifth row is the contribution ratio, the third row divided by the first row (or fourth divided by second).

mutation 15887(1.000)			crossover 8655(1.000)				triangulation 9758(1.000)			
[<<]	[≈]	[>>]	[<<]	[≤]	[≈]	[>>]	[<<]	[≤]	[≈]	[>>]
9326	5818	743	1004	2868	4246	532	579	2427	6214	543
(0.587	0.366	0.047)	(0.116	0.332	0.491	0.062)	(0.059	0.249	0.636	0.056)
109	990	205	19	97	739	60	5	111	1190	105
(0.007	0.062	0.013)	(0.002	0.011	0.085	0.007)	(0.001	0.011	0.122	0.011)
0.012	0.170	0.276	0.019	0.034	0.174	0.113	0.009	0.046	0.192	0.193

Table A9. Children relative fitness classification for Experiment GA-S1.

mutation 20473(1.000)			crossover 9064(1.000)				triangulation 11711(1.000)			
[<<]	[≈]	[>>]	[<<]	[≤]	[≈]	[>>]	[<<]	[≤]	[≈]	[>>]
16032	3273	1167	3082	876	3596	1511	3820	1386	4777	1728
(0.783	0.160	0.057)	(0.340	0.097	0.397	0.167)	(0.326	0.118	0.408	0.148)
89	328	63	33	30	298	69	28	49	446	69
(0.004	0.016	0.003)	(0.004	0.003	0.033	0.008)	(0.002	0.004	0.038	0.006)
0.006	0.100	0.054	0.011	0.034	0.083	0.046	0.007	0.035	0.093	0.040

Table A10. Children relative fitness classification for Experiment GA-DE.

mutation 33420(1.000)			crossover 15412(1.000)				triangulation 19261(1.000)			
[<<]	[≈]	[>>]	[<<]	[≤]	[≈]	[>>]	[<<]	[≤]	[≈]	[>>]
30112	2510	788	4110	5694	4657	944	3899	8372	6382	625
(0.901	0.075	0.024)	(0.267	0.370	0.302	0.061)	(0.202	0.434	0.331	0.032)
420	313	52	122	204	648	125	90	370	1134	86
(0.013	0.009	0.002)	(0.008	0.013	0.042	0.008)	(0.005	0.019	0.059	0.004)
0.014	0.125	0.066	0.030	0.036	0.139	0.132	0.023	0.044	0.178	0.138

Table A11. Children relative fitness classification for Experiment GA-D.

mutation 17054(1.000)			crossover 11015(1.000)				triangulation 12017(1.000)			
[<<]	[≈]	[>>]	[<<]	[≤]	[≈]	[>>]	[<<]	[≤]	[≈]	[>>]
13649	2791	606	3992	2849	3601	571	3523	3791	4318	395
(0.800	0.164	0.036)	(0.362	0.259	0.327	0.052)	(0.293	0.315	0.359	0.033)
217	363	51	96	97	459	78	69	161	654	56
(0.013	0.021	0.003)	(0.009	0.009	0.042	0.007)	(0.006	0.013	0.054	0.005)
0.016	0.130	0.084	0.024	0.034	0.127	0.137	0.020	0.042	0.151	0.142

Table A12. Children relative fitness classification for Experiment GA-4.

mutation 12093(1.000)			crossover 4842(1.000)				triangulation 6119(1.000)			
[<<]	[≈]	[>>]	[<<]	[≤]	[≈]	[>>]	[<<]	[≤]	[≈]	[>>]
10569	1200	323	1744	1510	1300	288	1592	2528	1742	258
(0.874	0.099	0.027)	(0.360	0.312	0.268	0.059)	(0.260	0.413	0.285	0.042)
147	191	35	43	43	216	27	33	114	323	29
(0.012	0.016	0.003)	(0.009	0.009	0.045	0.006)	(0.005	0.019	0.053	0.005)
0.014	0.159	0.108	0.025	0.028	0.166	0.094	0.021	0.045	0.185	0.112

Table A13. Children relative fitness classification for Experiment GA-F.

mutation 13933(1.000)			crossover 4151(1.000)				triangulation 6759(1.000)			
[<<]	[≈]	[>>]	[<<]	[≤]	[≈]	[>>]	[<<]	[≤]	[≈]	[>>]
12753	875	302	1286	1533	980	347	1705	3096	1765	201
(0.915	0.063	0.022)	(0.310	0.370	0.236	0.084)	(0.252	0.458	0.261	0.030)
203	103	26	30	68	173	43	63	198	461	45
(0.015	0.007	0.002)	(0.007	0.016	0.042	0.010)	(0.009	0.029	0.068	0.007)
0.016	0.118	0.086	0.023	0.044	0.177	0.124	0.037	0.064	0.261	0.224

Table A14. Children relative fitness classification for Experiment GA-F2.

$f_1(I)$	$f_2(I)$	$f_B(I)$	GA-1	GA-S1	GA-DE	GA-D	GA-4	GA-F	GA-F2
1. $n(\mathbb{P}(I)) = 1$	$d(I) = 0$	True	1678.37 \ominus	176.82 \ominus	195.35 \ominus	1101.14 \ominus	228.43 \ominus	233.27 \ominus	646.90 \ominus
2. $n(\mathbb{P}(I)) = 2$	$d(I) = 0$	True	352.27 \oplus	0.00 \ominus	40.03 \oplus	144.68 \oplus	22.07 \oplus	31.02 \oplus	32.89 \oplus
3. $n(\mathbb{P}(I)) = 3$	$d(I) = 0$	True	736.92 \oplus	215.63 \oplus	92.78 \oplus	656.16 \oplus	136.57 \oplus	145.75 \oplus	552.01 \oplus
4. $I \in [\gg]$	$d(I) = 0$	True	3086.23 \oplus	193.47 \oplus	11.85 \oplus	172.65 \oplus	109.81 \oplus	50.53 \oplus	97.78 \oplus
5. $I \in [\simeq]$	$d(I) = 0$	True	2384.30 \oplus	1766.64 \oplus	1429.42 \oplus	3566.00 \oplus	1745.43 \oplus	1513.70 \oplus	1698.94 \oplus
6. $I \in [\leq]$	$d(I) = 0$	True	8.22 \ominus	291.79 \ominus	0.08 \ominus	47.13 \ominus	50.13 \ominus	16.82 \ominus	0.05 \oplus
7. $I \in [\ll]$	$d(I) = 0$	True	6373.92 \ominus	1482.62 \ominus	1314.95 \ominus	2233.94 \ominus	1283.65 \ominus	923.74 \ominus	1162.42 \ominus
8. $n(\mathbb{P}(I)) = 2$	$d(I) = 0$	$n(\mathbb{P}(I)) \geq 2$	0.50 \ominus	62.38 \ominus	1.06 \ominus	29.02 \ominus	12.05 \ominus	7.15 \ominus	40.75 \ominus
9. $n(\mathbb{P}(I)) = 3$	$d(I) = 0$	$n(\mathbb{P}(I)) \geq 2$	0.50 \oplus	62.38 \oplus	1.06 \oplus	29.02 \oplus	12.05 \oplus	7.15 \oplus	40.75 \oplus
10. $n(\mathbb{P}(I)) = 2$	$I \in [\gg]$	$I \in \mathbb{E}$	410.39 \oplus	31.79 \oplus	13.00 \oplus	179.86 \oplus	64.28 \oplus	18.81 \oplus	144.85 \oplus
11. $n(\mathbb{P}(I)) = 3$	$I \in [\gg]$	$I \in \mathbb{E}$	410.39 \ominus	31.79 \ominus	13.00 \ominus	179.86 \ominus	64.28 \ominus	18.81 \ominus	144.85 \ominus
12. $n(\mathbb{P}(I)) = 2$	$I \in [\gg]$	$d(I) = 0$	69.73 \oplus	17.64 \oplus	3.72 \oplus	37.14 \oplus	10.15 \oplus	0.26 \oplus	17.27 \oplus
13. $n(\mathbb{P}(I)) = 2$	$I \in [\simeq]$	$d(I) = 0$	177.77 \ominus	0.11 \oplus	1.20 \ominus	0.03 \oplus	0.72 \ominus	4.60 \oplus	1.43 \oplus
14. $n(\mathbb{P}(I)) = 3$	$I \in [\gg]$	$d(I) = 0$	340.94 \ominus	19.05 \ominus	2.49 \ominus	23.71 \ominus	9.29 \ominus	3.77 \ominus	10.90 \ominus
15. $n(\mathbb{P}(I)) = 3$	$I \in [\simeq]$	$d(I) = 0$	368.68 \oplus	22.80 \oplus	7.69 \oplus	100.03 \oplus	20.56 \oplus	5.72 \oplus	42.80 \oplus
16. $I \equiv 7 \pmod{10}$	$d(I) = 0$	True	1.73 \ominus	1.38 \ominus	0.41 \ominus	1.00 \ominus	0.98 \oplus	0.00 \ominus	0.02 \ominus
17. $I \equiv 13 \pmod{100}$	$d(I) = 0$	True	1.05 \oplus	0.69 \oplus	0.06 \oplus	0.08 \ominus	0.43 \ominus	0.08 \oplus	1.11 \oplus

Table A15. Chi-squared test of statistical independence of predicates. For each pair of experiment (columns) and three predicates $f_1(I), f_2(I), f_B(I)$, the table shows the X^2 statistics of the null hypothesis “predicates $f_1(I)$ and $f_2(I)$ are statistically independent for the population of individuals that satisfy predicate $f_B(I)$.” Here, $\mathbb{E} \equiv \{I | n(\mathbb{P}(I)) \geq 2\} \cap ([\gg] \cup [\simeq])$. \oplus denotes the positive correlation and \ominus denotes the negative correlation.

$f_1(I)$	$f_2(I)$	$f_B(I)$	GB-333-0	GB-333-1	GB-333-2
1. $n(\mathbb{P}(I)) = 1$	$d(I) = 0$	True	189.24 \ominus	309.78 \ominus	374.03 \ominus
2. $n(\mathbb{P}(I)) = 2$	$d(I) = 0$	True	17.50 \oplus	1.38 \oplus	15.90 \oplus
3. $n(\mathbb{P}(I)) = 3$	$d(I) = 0$	True	107.73 \oplus	284.28 \oplus	255.24 \oplus
4. $I \in [\gg]$	$d(I) = 0$	True	19.56 \oplus	28.84 \oplus	41.97 \oplus
5. $I \in [\simeq]$	$d(I) = 0$	True	455.57 \oplus	517.15 \oplus	1024.86 \oplus
6. $I \in [\leq]$	$d(I) = 0$	True	0.05 \ominus	1.67 \ominus	8.49 \ominus
7. $I \in [\ll]$	$d(I) = 0$	True	333.89 \ominus	514.23 \ominus	794.08 \ominus
8. $n(\mathbb{P}(I)) = 2$	$d(I) = 0$	$n(\mathbb{P}(I)) \geq 2$	9.69 \ominus	67.58 \ominus	38.17 \ominus
9. $n(\mathbb{P}(I)) = 3$	$d(I) = 0$	$n(\mathbb{P}(I)) \geq 2$	9.69 \oplus	67.58 \oplus	38.17 \oplus
10. $n(\mathbb{P}(I)) = 2$	$I \in [\gg]$	$I \in \mathbb{E}$	207.54 \oplus	70.91 \oplus	138.99 \oplus
11. $n(\mathbb{P}(I)) = 3$	$I \in [\gg]$	$I \in \mathbb{E}$	207.54 \ominus	70.91 \ominus	138.99 \ominus
12. $n(\mathbb{P}(I)) = 2$	$I \in [\gg]$	$d(I) = 0$	43.23 \oplus	12.05 \oplus	70.57 \oplus
13. $n(\mathbb{P}(I)) = 2$	$I \in [\simeq]$	$d(I) = 0$	1.47 \oplus	17.39 \oplus	0.22 \oplus
14. $n(\mathbb{P}(I)) = 3$	$I \in [\gg]$	$d(I) = 0$	44.86 \ominus	18.46 \ominus	60.99 \ominus
15. $n(\mathbb{P}(I)) = 3$	$I \in [\simeq]$	$d(I) = 0$	3.15 \oplus	7.75 \oplus	0.12 \oplus
16. $I \equiv 7 \pmod{10}$	$d(I) = 0$	True	3.77 \ominus	0.47 \oplus	2.74 \oplus
17. $I \equiv 13 \pmod{100}$	$d(I) = 0$	True	0.63 \ominus	4.27 \ominus	0.23 \ominus

Table A16. The same table for GB-333-*

References

- [1] M. Frigo and S.G. Johnson. The design and implementation of FFTW3. *Proceedings of the IEEE*, 93(2):216231, 2005.
- [2] R. Clint Whaley, A. Petitet, and J.J. Dongarra. Automated empirical optimizations of software and the ATLAS project. *Parallel Computing*, 27(1-2):335, 2001.
- [3] M. Puschel, J.M.F. Moura, J.R. Johnson, D. Padua, M.M. Veloso, B.W. Singer, J. Xiong, F. Franchetti, A. Gacic, Y. Voronenko, et al. SPIRAL: code generation for DSP transforms. *Proceedings of the IEEE*, 93(2):232275, 2005.
- [4] Kaushik Datta, Mark Murphy, Vasily Volkov, Samuel Williams, Jonathan Carter, Leonid Oliker, David Patterson, John Shalf, and Katherine Yelick. Stencil computation optimization and auto-tuning on state-of-the-art multicore architectures. In *Proceedings of the 2008 ACM/IEEE conference on Supercomputing*, SC '08, page 4:14:12, Piscataway, NJ, USA, 2008. IEEE Press.
- [5] Naoya Maruyama, Tatsuo Nomura, Kento Sato, and Satoshi Matsuoka. Physis: an implicitly parallel programming model for stencil computations on large-scale GPU-accelerated supercomputers. In *Proceedings of 2011 International Conference for High Performance Computing, Networking, Storage and Analysis*, SC '11, page 11:111:12, New York, NY, USA, 2011. ACM.
- [6] P.W. Trinder, H.W. Loidl, and R.F. Pointon. Parallel and distributed haskells. *Journal of Functional Programming*, 12(5):469510, 2002.
- [7] M. Chakravarty, G. Keller, R. Lechtchinsky, and W. Pfannenstiel. Nepalnested data parallelism in haskell. *Euro-Par 2001 Parallel Processing*, page 524534, 2001.
- [8] S.P. Jones, R. Leshchinskiy, G. Keller, and M.M.T. Chakravarty. Harnessing the multicores: Nested data parallelism in haskell. In *FSTTCS*, volume 2, page 383414, 2008.
- [9] M.M.T. Chakravarty, G. Keller, S. Lee, T.L. McDonell, and V. Grover. Accelerating haskell array codes with multicore GPUs. In *Proceedings of the sixth workshop on Declarative aspects of multicore programming*, page 314, 2011.
- [10] G. Mainland and G. Morrisett. Nikola: embedding compiled GPU functions in haskell. In *Proceedings of the third ACM Haskell symposium on Haskell*, page 6778, 2010.
- [11] Zachary DeVito, Niels Joubert, Francisco Palacios, Stephen Oakley, Montserrat Medina, Mike Barrientos, Erich Elsen, Frank Ham, Alex Aiken, Karthik Duraisamy, Eric Darve, Juan Alonso, and Pat Hanrahan. Liszt: a domain specific language for building portable mesh-based PDE solvers. In *Proceedings of 2011 International Conference for High Performance Computing, Networking, Storage and Analysis*, SC '11, page 9:19:12, New York, NY, USA, 2011. ACM.
- [12] Takashi Shimokawabe, Takayuki Aoki, Chiashi Muroi, Junichi Ishida, Kohei Kawano, Toshio Endo, Akira Nukada, Naoya Maruyama, and Satoshi Matsuoka. An 80-Fold speedup, 15.0 TFlops full GPU acceleration of Non-Hydrostatic weather model ASUCA production code. In *Proceedings of the 2010 ACM/IEEE International Conference for High Performance Computing, Networking, Storage and Analysis*, SC '10, page 111, Washington, DC, USA, 2010. IEEE Computer Society.
- [13] Takashi Shimokawabe, Takayuki Aoki, Tomohiro Takaki, Toshio Endo, Akinori Yamanaka, Naoya Maruyama, Akira Nukada, and Satoshi Matsuoka. Peta-scale phase-field simulation for dendritic solidification on the TSUBAME 2.0 supercomputer. In *Proceedings of 2011 International Conference for High Performance Computing, Networking, Storage and Analysis*, SC '11, page 3:13:11, New York, NY, USA, 2011. ACM.
- [14] T. Hoshino, H.S. Stone, and S. Goldman. *PAX Computer; High-Speed Parallel Processing and Scientific Computing*. Addison-Wesley Longman Publishing Co., Inc., 1989.
- [15] J. Lee and M. Sato. Implementation and performance evaluation of xcalablemp: A parallel programming language for distributed memory systems. In *Parallel Processing Workshops (ICPPW), 2010 39th International Conference on*, page 413420, 2010.
- [16] C. McBride and R. Paterson. Functional pearl: Applicative programming with effects. *Journal of functional programming*, 18(1):113, 2008.

- [17] G. Keller, M.M.T. Chakravarty, R. Leshchinskiy, S. Peyton Jones, and B. Lippmeier. Regular, shape-polymorphic, parallel arrays in haskell. *ACM SIGPLAN Notices*, 45(9):261272, 2010.
- [18] J. Gibbons and B.C.S. Oliveira. The essence of the iterator pattern. *Journal of Functional Programming*, 19(3-4):377402, 2009.
- [19] M. Erwig. Functional programming with graphs. In *ACM SIGPLAN Notices*, volume 32, page 5265, 1997.
- [20] M. Erwig. Inductive graphs and functional graph algorithms. *Journal of Functional Programming*, 11(05):467492, 2001.
- [21] T. Sheard and S.P. Jones. Template meta-programming for haskell. In *Proceedings of the 2002 ACM SIGPLAN workshop on Haskell*, page 116, 2002.
- [22] Dylan Thurston, Henning Thielemann, and Mikael Johansson. numeric-prelude: An experimental alternative hierarchy of numeric type classes. <http://hackage.haskell.org/package/numeric-prelude>, 2012.
- [23] Ralf Lmmel and Simon Peyton Jones. Scrap your boilerplate: a practical design pattern for generic programming. *SIGPLAN Not.*, 38(3):2637, January 2003.
- [24] Koji Hukushima and Koji Nemoto. Exchange monte carlo method and application to spin glass simulations. *Journal of the Physical Society of Japan*, 65:1604–1608, 1996.
- [25] Jos A. Garca Gutierrez, Carlos Cotta, and Antonio J Fernandez-Leiva. Evolutionary computation in astronomy and astrophysics: A review. *arXiv:1202.2523*, February 2012.
- [26] A. Eiben, P. Rau, and Z. Ruttkay. Genetic algorithms with multi-parent recombination. *Parallel Problem Solving from NaturePPSN III*, page 7887, 1994.
- [27] SN Sivanandam and SN Deepa. *Introduction to genetic algorithms*. Springer Verlag, 2007.
- [28] A. Eiben, C. Van Kemenade, and J. Kok. Orgy in the computer: Multi-parent reproduction in genetic algorithms. *Advances in Artificial Life*, page 934945, 1995.
- [29] S. Tsutsui, M. Yamamura, and T. Higuchi. Multi-parent recombination with simplex crossover in real coded genetic algorithms. In *Proceedings of the Genetic and Evolutionary Computation Conference*, volume 1, page 657664, 1999.
- [30] Eleuterio F. Toro. *Riemann Solvers And Numerical Methods for Fluid Dynamics: A Practical Introduction*. Springer-Verlag, 3 edition, June 2009.
- [31] P.K. Sweby. High resolution schemes using flux limiters for hyperbolic conservation laws. *SIAM journal on numerical analysis*, page 9951011, 1984.
- [32] E. F. Toro, M. Spruce, and W. Speares. Restoration of the contact surface in the HLL-Riemann solver. *Shock Waves*, 4(1):25–34, July 1994.
- [33] H.Y. Schive, U.H. Zhang, and T. Chiueh. Directionally unsplit hydrodynamic schemes with hybrid MPI/OpenMP/GPU parallelization in AMR. *Arxiv preprint arXiv:1103.3373*, 2011.
- [34] M. de la Asuncina, M.J. Castroc, ED Fernandez-Nietob, J.M. Mantasa, S.O. Acostac, and J.M. Gonzalez-Vidad. Efficient GPU implementation of a two waves WAF method for the two-dimensional one layer shallow water system on structured meshes.
- [35] Philippe Charles, Christian Grothoff, Vijay Saraswat, Christopher Donawa, Allan Kielstra, Kemal Ebcioglu, Christoph von Praun, and Vivek Sarkar. X10: an object-oriented approach to non-uniform cluster computing. *SIGPLAN Not.*, 40(10):519538, October 2005.
- [36] B.l. Chamberlain, D. Callahan, and H.p. Zima. Parallel programmability and the chapel language. *International Journal of High Performance Computing Applications*, 21(3):291–312, 2007.
- [37] Jon K Nilsen, Xing Cai, Bjrn Hyland, and Hans Petter Langtangen. Simplifying the parallelization of scientific codes by a function-centric approach in python. *Computational Science & Discovery*, 3(1):015003, September 2010.